# Research on a Vision System for Autonomous Inspection Robots
( )

Alireza Ahrary

Supervisor: Prof. Masumi Ishikawa

A thesis submitted to the Kyushu Institute of Technology
in partial fulfillment of the requirement for
the degree of Doctor of Philosophy

Department of Brain Science and Engineering
Graduate School of Life Science and Systems Engineering
Kyushu Institute of Technology, Japan

March 2007

# Contents

# List of Figures

iv

# List of Tables

# Acknowledgements

There are many people to thank for their support and encouragement, without whom this thesis would not have been born.

First of all, I would like to express my appreciation to my supervisor, Prof. Masumi Ishikawa, whose support and guidance made my thesis work possible. He has been actively interested in my work and has always been available to advise me. I am very grateful for his patience, enthusiasm, and immense knowledge that, taken together, made him a great mentor. I also thank my official referees, Prof. Kazuo Ishii and Prof. Hiroyuki Miyamoto for their valuable and constructive criticism during the preparation of the manuscript.

I am also greatly indebted to many teachers in the past: Prof. Jun Kumagai and Dr. Yasushi Inomata (Kitakyushu National College of Technology) for getting me interested in Image Processing. Prof. Noriyoshi Kambayashi and Dr. Pavol Zavarsky (Nagaoka University of Technology) for guiding me to taste one of interesting area in Image Processing, Digital Watermarking. Prof. Hisakazu Kikuchi (Niigata University) for teaching and helping me to stand in the right way. Much respect to Dr. Toshiro Yamashita (Kitakyushu City Office) for assisting and motivated me to start my PhD.

This research was funded by the Organization for Small and Medium Enterprises and Regional Innovation, JAPAN (SMRJ). I thankfully acknowledge the cooperation with the project partners, Yaskawa Electric Co., Kyushu Keisokuki Co., Nihon Tecmo Ltd. and FAIS. I am also grateful to all members of the former GMD-JRL and FAIS Robotics Development Support Office, Prof. Thomas Christaller, Dr. Saeed Shiry, Masayoshi Miki, Yoshikazu Mikuriya, Amir A.F. Nassiraei, Yoshinori Kawamura, Kenji Kondo, Mayumi Oda and Miki Takaba for their supporting throughout these three years.

I would like to thank deeply my family. My parents, for giving me life in the first place, for educating me and for unconditional support and encouragement to pursue my interest. My brother and my sisters for encouraging me throughout past years.

Last, but not least, I would like to extend my deepest gratitude to my wife, for all supports that she gave me during the years. She always has provided unwavering love and encouragement. Thank you for believing in me.

<div align="right">

Alireza Ahrary
2007/03

</div>

**Abstract**

Pipe walls in sewer systems are prone to be damaged due to aging, traffic and chemical reactions, through which inflow such as rainwater and groundwater seeps into pipe systems. Regional city government reports state that this inflow amounts to approximately 30% of the total flow. In addition to the inflow of groundwater into the sewer pipes, outflow from damaged systems also occurs, contaminating the surrounding environment.

Conventional inspection of a sewer pipe system is carried out using a cable-tethered robot with an onboard video camera system. This robot is connected to the outside of sewer system by a cable. The cable is used for energy supply, transmission of commands from a human operator to the device, data transmission back to an operator, a life-line in case the device gets stuck in the pipe, and measuring the distance traveled. An operator remotely controls the movement of the robot and the video system. By this video-supported visual inspection, any notable damages or abnormalities are recorded in video stream. The reliability of this system depends on the experience of an operator. The system is also prone to human error, and tends to be time consuming and expensive. Consequently, effective autonomous robot capable of online identification and extraction of objects of interest such as cracks from sensory signals is of immediate concern.

Based on the above, we design a prototype autonomous mobile robot, KANTARO, for inspecting sewer pipes. It is able to move autonomously in 200-300mm diameter sewer pipes, to smoothly turn 90 degrees at a junction, and to go down a step. KANTARO carries all required resources such as a control unit, a camera, a 2D laser and an IR sensor. Damages or abnormalities in sewer pipes are detected based on recorded sensory data. In this thesis, I focus on an automated fault detection system, navigation system, and stereo vision system for autonomous inspection robots such as KANTARO.

Robust detection of cracks and other faults in sewer pipes based on sensory data is another important challenge. However, all related previous works focused on specific types of faults in pipes, hence were unable to detect multiple types of faults. Accordingly, a truly automated fault detection system is currently not available in the real world. I propose a method for detecting faulty areas based on images, and an automated intelligent system designed to facilitate diagnosis of faulty areas in a sewer pipes system. The system utilizes image analysis and efficient techniques for providing the location and the number of faults in a sewer pipe system. In contrast to the conventional

manual system, the proposed system can automatically detect faults and move in real time. Its detection performance is 100%, when the false positive rate is 34%. This ratio is said to be acceptable for sewer inspection, and the reduction of time and cost is also realized.

Another central issue in developing an autonomous sewer robot is its navigation. Navigation of an autonomous sewer robot based on a map of sewer pipe system is not applicable as it is, because large slips in sewer pipes tend to produce erroneous odometry information, causing unreliable localization. It is to be noted that data from Global Positioning System (GPS) are not available in underground sewer pipe systems. Accordingly, an autonomous robot has to estimate the current position based on local features.

Navigation of an autonomous sewer robot is composed of the following tasks. Firstly, estimation of the current position based on salient local features such as manholes, inlets and pipe joints. Secondly, finding a path. Thirdly, following the path in the real sewer pipe system. Resulting maps of the sewer pipe system describe pipes, manholes and other local features, which contribute to localization. I propose a method for navigation of an autonomous inspection robot based on fusion of single camera images and IR sensor data. It is capable of self localization, which cannot be done by the conventional methods. We also conduct experiments for sewer robot navigation in a dry sewer test field at FAIS-RDSO, Kitakyushu. They succeed in detecting local features and show high performance of self localization by using sensory information. In additional to using a single camera in the above proposed methods, I also use a stereo camera to see the performance of stereo vision for navigation, which is described as follows.

Stereo matching is an essential issue in computer vision. Recently, many stereo matching algorithms based on segmentation, graph cuts and so on have been proposed. Because the disparities change continuously in sewer environment, these methods are not applicable to sewer systems and are computationally expensive. I propose a cooperative stereo matching algorithm using Sum of Squared Differences (SSD) and Linear Computation (LC) measures, which can be implemented in a real-time system. It is a robust algorithm for sewer inspection in robot vision. The algorithm produces an easy-to-understand distance map of the sewer, emphasizing the feature region. The computational time by this algorithm is about 1/5 compared with that by other algorithms such as the conventional SSD. In order to reduce the computational time, I also propose a fast stereo matching algorithm using interpolation. The computational time by the proposed algorithm is only 1/20 of those by the conventional algorithms such as the SSD. Hence it is suitable for our real-time sewer vision system.

The above stereo matching algorithm is utilized for proposing another method for navigation which is based on stereo camera images and laser scanner data. Experimental results of self localization show high performance in providing the appropriate distance. We also design a new mobile laser scanner for KANTARO. The locations of landmarks in sewer pipe system are estimated successfully based on measurements. The laser scanner is fast enough to continuously scan relevant pipe sections in the presence of landmarks, while the KANTARO moves at ordinary inspection speed of less than 15cm/s. Also moving the KANTARO in our sewer test field by using the proposed method is done successfully.

# Chapter 1

# Introduction

Pipe walls in sewer systems are prone to be damaged due to aging, traffic and chemical reactions, through which inflow such as rainwater and groundwater seeps into pipe systems. Regional city government reports state that this inflow amounts to approximately 30% of the total flow. In addition to the inflow of groundwater into the sewer pipes, outflow from damaged systems also occurs, contaminating the surrounding environment.

Conventional inspection of a sewer pipe system is carried out using a cable-tethered robot with an onboard video camera system. This robot is connected to the outside of sewer system by a cable. The cable is used for energy supply, transmission of commands from a human operator to the device, data transmission back to an operator, a life-line in case the device gets stuck in the pipe, and measuring the distance traveled. An operator remotely controls the movement of the robot and the video system. By this video-supported visual inspection, any notable damages or abnormalities are recorded in video stream. The reliability of this system depends on the experience of an operator. The system is also prone to human error, and tends to be time consuming and expensive. Consequently, effective autonomous robot capable of online identification and extraction of objects of interest such as cracks from sensory signals is of immediate concern.

The purpose of this thesis is to elucidate the systems for detecting the faults automatically and navigation system for autonomous sewer inspection robot. The proposed systems can solve the "real-world" problems in civil robots, such as, support the operator and reduce the human error, tends to time and cost reduction.

In chapter 2, I will summarize the sewer systems and conventional sewer robots and sewer sensors. Also, conventional inspection methods and their difficulties will discuss here. An berif introduction to a prototype autonomous mobile robot, KANTARO, will located at the end. In chapter

3, I will introduce a method for detecting faulty areas based on images, and propose an automated intelligent system designed to facilitate diagnosis of faulty areas in a sewer pipes system. The experimental results and conclusions of proposed method is explained at the end of this chapter.

In chapter 4, a navigation method based on single camera and IR sensors is described. The proposed method is capable of self localization, which cannot be done by conventional methods. Experimental results shows a high performance in a dry sewer test field. To see the perfomance of stereo vision, I also proposed a methed for navigation by using a stereo camera, which is described at chapter 5.

In chapter 5, first, I will explain two differents stereo matching algorithms. First stereo matching algorithm is utilized for proposing another method for navigation which is based on stereo camera images and laser scanner data. The proposed navigation method is explained in section 5.5.

In chapter 6, I will describe the conclusions from the results of these proposed methods.

# Chapter 2

# Overview of sewer systems and inspection systems

## 2.1   Introduction

The usage of tethered, remotely controlled robot platforms in sewer pipes has become widely accepted. Research and development in engineering have moved the original application field of merely visual inspection to manipulative tasks such as the actual repair of pipe sections, installation of cable, e.g. for communication.

Despite all engineering advances in the mechanical design of the platforms and improvements of the video equipment, these efforts are directed to increase the quality of the data provided to the human operator. Yet the potential for automatic processing and data analysis in combination with hardware platform, as well as the application of IT technology for the development of an integrated sewer information system is neglected.

In this chapter, we being with the introduction of the legal framework together with the present inspection method, in which environment sewer inspection is embedded. Further, we will point out critical issues involved with the present inspection method.

Sewer systems are prone to damages due to aging, traffic, geological change, to name a few. Due to these damages, the groundwater is increasingly contaminated. Furthermore, heavy rainfall events may lead to inroad of the systems, resulting in overflow. In the case of separate sewer system as widely present in Japan (Table 2.1), this results in the undesired mixture of wastewater and rainwater. Thus, in order to ensure an optimal functioning sewer system, extensive inspection is necessary. Preceding repair are extensive qualified diagnostic measurement. Tethered mobile robots used for visual

inspection in municipal and industrial sewer networks are one example. Beyond this classic task of application of the tethered robot as an extended tool of the human operator, new fields have emerged. Due to ongoing research and development of the mechanical design, tethered robots are now able to perform repair tasks with varying degree of complexity. Another emerging fields of application are the installation of communication cable in the sewersystem as well as the encasement of inner pipewalls during renovation or repair [1].

Table 2.1: Division of sewer system.

| separate sewer (sanitary sewer) | separate sewer (rainwater) | combined sewer |
|---|---|---|
| 73% | 5% | 22% |

In Japan, matters regarding sewerpipes are regulated by the Sewage Water Law. The municipal governments as owners of the facilities are responsible for installation and maintenance of the public sewersystem. In practice, authorities such as the construction bureau will authorize local companies to conduct inspections and after deciding upon the necessity also outsource the repair.

Although inspection cycles are clearly defined and also governed in the The sewage system book, in reality, inspections are done after the occurrence of noticeable damages. Due to limitations in budget and equipment, the given inspection intervals are not strictly adhered to. This can also be clearly seen by comparison of actual inspected distance, 77km (Table 2.2) with total length of applicable sewer pipes, 3,220,053m (Table 2.3), for the financial year 2000. This gives us a ration of 0.0017%.

Table 2.2: Inspected sewer length per year at Kitakyushu city.

| Year | 1996 | 1997 | 1998 | 1999 | 2000 | 2001 | 2002 |
|---|---|---|---|---|---|---|---|
| Length (m) | 46,374 | 45,103 | 59,786 | 52,922 | 53,956 | 53,019 | 77,711 |

We have to distinguish between two different types of inspection. For sewerpipe systems with an inner diameter larger than 800mm, human inspection is possible and conducted. The above mentioned tethered robot inspection platforms are used for pipes with a diameter less than 800mm.

---

[1]Most of the materials presented in this chapter have been selected from the material provided by "Steinbeis Japan Inc., Kitakyushu Foundation for the Advancement on Industry, Science and Technology," March 2002.

Table 2.3: Present condition of sewer pipe length (diameter < 800mm) at Kitakyushu city, (financial year 2000).

| Diameter (mm) | Length (m) |
|:---:|:---:|
| 0 | 18,692 |
| 150 | 210,424 |
| 200 | 2,074,502 |
| 250 | 329,528 |
| 300 | 144,505 |
| 350 | 81,914 |
| 380 | 18,099 |
| 400 | 64,869 |
| 450 | 61,921 |
| 480 | 102 |
| 500 | 65,141 |
| 600 | 85,373 |
| 700 | 64,983 |
| Sum (m) | 3,220,053 |

Both inspection procedures common is the acquisition of damages by the human inspector, either on loci or by means of video equipment.

Based on the above information, manual inspection is done at maximum 77km/year which would take more than 40 years to complete all of the 3220km of pipes in Kitakyushu. In additional, reliability of the current inspection method is depends on experience of an operator and it is also prone to human error. Accordingly, an effective autonomous robot capable of online identification and extraction of objects of interest such as cracks from sensory signals is of immediate concern.

## 2.2   Sewer pipe system

A property owner's sewer pipes are called service laterals and are connected to larger local main and regional trunk lines. Service laterals run from the connection at the home to the connection with the public sewer (including the area under the street). These laterals are the responsibility of the property owner and must be maintained by the property owner. Many city agencies have adopted ordinances requiring maintenance of service laterals. Operation and maintenance of local and regional sewer lines are the responsibility of the city sewer/public works departments and public sewer districts [1].
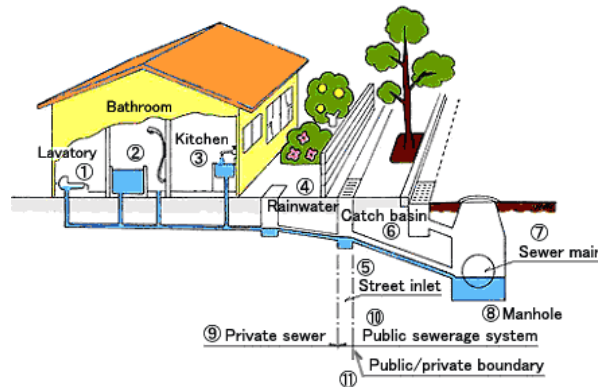
Figure 2.1: Sewer pipe system in residental area[2].

## 2.3 Conventional sewer robots

**PIRAT**

PIRAT (Pipe Inspection Real-Time Assessment Technique) is a semi autonomous tethered robot for the quantitative and automatic assessment of sewer condition [3]. The PIRAT sewer inspection system has been developed between 1993 and 1996 within a joint project of the Manufacturing Systems and Automation Division of Australian CSIRO Manufacturing Science and Technology and Melbourne Water. Just like a conventional sewer inspection device, PIRAT (Fig. 2.2) is deployed to a sewer, and tele-operated from a surveillance unit via a cable by a human operator. The maximum cable length of 250m gives PIRAT a fair operating range. The added value of the PIRAT system is its ability to perform automatic evaluation of its sensory data.

PIRAT's innovative instrument system contains a video camera and a laser scanner. For flooded sewers, the latter can be substituted by a sonar scanner, but at the price of less resolution and inspection speed. In 600mm sewer pipes and at PIRAT's usual inspection speed, the laser scanner produced a resolution of about 1.5mm radially and 4 mm axially and circumferentially.

The sensory data are evaluated by means of PIRAT's interpretation system, which is an expert system that runs on a Sun workstation in the mobile surveillance unit. From both types of scanner data, the interpretation system generated in a first step a three-dimensional model of the scanned sewer pipe section. In a second step, the interpretation system uses techniques from Artificial Intelligence to detect and classify damages on the basis of the
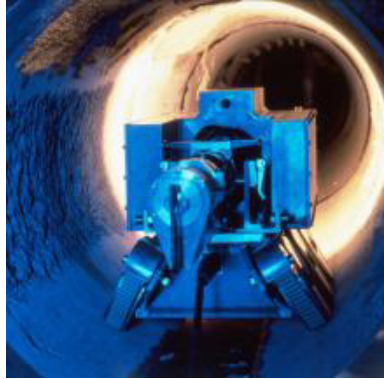
Figure 2.2: The automated video inspection platform, PIRAT[4].

three-dimensional model data. The result is a sewer condition assessment report that is readable for the human operator.

**KARO**

KARO (Kanalroboter - German for sewer robot) is an experimental semi-autonomous carrier for sewer inspection sensory equipment [5],[6]. It was developed by a group of research institutes and some industrial partners in Germany. The project was partly funded by the German Ministry for Research and Education (BMBF).

The monolithic KARO robot prototype (see Fig. 2.3) resembles much a standard non-autonomous sewer inspection robot, and it is tethered via a cable to a surveillance unit. Using inclinometers and an on-board control program, KARO is able to automatically correct for tilt in its pose and wheel slippage when driving inside a sewer pipe, thus freeing the human operator from this crucial control task.

The main innovation of KARO is its wide range of novel inspection and navigation sensors, namely, a microwave sensor and a 3D optical sensor, complementing the standard video camera and some ultrasound transducers. The method for 3D measurement of hollow spaces using axial symmetric structured infrared light has been patented. It is applied for measuring pipe deformations, larger pipe cracks and obstacles inside the pipe, the latter being detected early by the US transducers. The microwave sensors are aimed at detecting leakages.

KARO has been continued as an internal research project within Fraunhofer IITB at least until 2000. Most recent research deals with fuzzy methods for data fusion of inspection sensors.

7
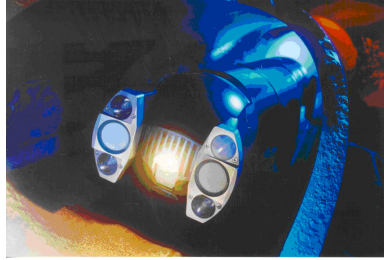
Figure 2.3: The multi sensorial sewer inspection robot prototype, KARO.

## KURT

The development of the experimental sewer robot test platform KURT (Kanal-Untersuchungs-Roboter-Testplattform) started at the former GMD - now Fraunhofer - institute AIS in 1995 [7]. KURT is a six-wheeled autonomous un-tethered robot of approximate dimensions $30 \times 45 \times 30$cm.

KURT version 1 has been successfully employed for navigating autonomously in a dry sewer test net at the premises of the Fraunhofer campus in Sankt Augustin. To achieve this, the robot is provided with a map of the test net, representing the topology of the 80m of sewer pipes and the nine manholes in between, with a start position (number of a manhole) and a goal manhole. The robot can determine the sequence of manholes or pipe junction types, respectively that it should pass on its path from start to goal. Since all pipe junctions inside the sewer test net are ground level connections, the robot is mechanically able to perform turns at such junctions. With its pivoted ultrasound sensor, KURT1 is able to classify the type of a pipe junction, i.e. whether it is L-shaped, X-shaped, or T-shaped. A special patented method for navigation under uncertainty enables KURT1 to detect and correct errors due to false classification or due to errors while performing turns at pipe junctions [8]. This work has been complemented by a method for probabilistic mapping of objects, like landmarks in the sewer [9].

Since its very first version, the KURT type robot platform has been further developed for indoor applications. The current version KURT2 can be equipped with a variety of sensors. The standard configuration includes inclinometers and sensors for odometry, either infrared or ultrasound distance transducers for obstacle detection, and optional bumpers. Fig. 2.4 shows a KURT2 system with a custom mounted 2D laser distance scanner and a notebook computer "Toughbook" as CPU. Alternatively, an industry standard PC/104+ CPU can be provided.

Figure 2.4: The commercial research robot platform, KURT2.

## MAKRO

MAKRO (Mehrsegmentiger Autonomer KanalROboter/multi-segmented autonomous sewer robot) is the prototype of a fully autonomous, un-tethered, self-steering articulated robot platform (Fig. 2.5). It is designed for autonomous navigation in roughly cleaned sewer pipes within a diameter range of 300 to 600mm at dry weather conditions.



Figure 2.5: Automated inspection platform, MAKRO.

MAKRO's case design, consisting of six segments connected by five motor-driven active joints, allows for simultaneously climbing a step and turning, e.g. at a junction consisting of a 600mm pipe and a branching 300mm pipe with equal top levels. MAKRO's autonomy and its kinematic abilities extend its potential mission range enormously, compared to conventional inspection equipment that is limited by the cable and poor kinematics [10]. MAKRO carries all the needed resources on-board. Standard NiCd batteries provide

the power for its 21 motors, the sensors, and the electronics, including an industry standard PC104 computer system and seven micro controllers [11], allowing for an autonomous uptime of about two hours.

The robot MAKRO has been developed by a German group of two research institutes and two industrial partners. The MAKRO project was funded partly by the German Ministry for Research and Education (BMBF) between 1997 and 2000. Since 2001, the MAKRO project is being continued as internal projects at Fraunhofer AIS and FZI [12].

## 2.4   Sewer sensors

In this section, we review innovative sensors and sensor interpretation methods for sewer maintenance. The range of the depicted sensors ranges from widely applicable sensors such as compasses for navigation, to general usage sensor such as laser scanners up to especially for the application in sewer system developed ground penetrating sensors. Besides sensor systems, innovative methods of sewer maintenance, states of sewer pipes are of interest. The fusion of these innovative sensors and application methods will ensure that not only exhibited damage in the pipe in a narrow sense like a leak or crack or a blockage, but are potential heralds of a growing damage, like a bent or twisted pipe segment are successfully identified.

**Laser scanners**

Laser scanners are a technology that is in broad use in autonomous robots in general. Originally, they were developed as security sensors for surveying free space in production processes (such as protected areas around dangerous machines). For indoor applications, they are available in many different varieties at a highly developed technological level. The general principle is to measure by run-time of a laser beam the distance from a laser source to target objects. In scanners, the laser beam is deflected at different angles, measuring distances along a plane or half-plane, depending on the rotation and form of the deflecting mirror. The accuracy of the individual measurements is in the order of 1mm, depending on the measuring device and the distance.

The application principle for sewer inspection is to mount the scanner such that it scans radially the inner side of a pipe wall, see Fig. 2.6. If the inspection device moves along the pipe while measuring, the laser beam measures along a spiral on the pipe inside, where the resolution of the spiral depends on the turn rate of the reflection mirror and the speed of horizontal motion of the inspection device, typical turn rates being 1-2 turns per second.

As a result, a model of the pipe geometry can be directly acquired, which makes possible to detect deformations within the accuracy and resolution of the measurement principle.

Recently, prototypes of such sewer laser scanners have become available on the market. We mention two such systems here. Due to the precision and simplicity of the measurement principle and due to the simplicity of data interpretation, we expect laser scanners to become important sensors on fully autonomous or semi-autonomous sewer inspection robots.
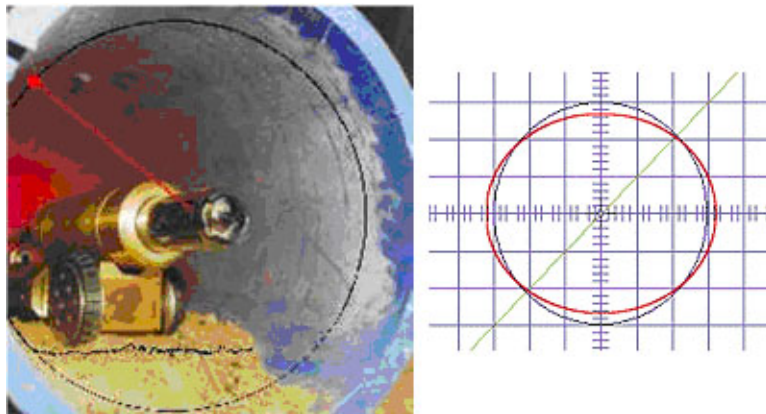


Figure 2.6: OMC pipe profiler (City University of London).
Measured distances (red) overlayed with the circle (blue) that would represent the ideal pipe inside (profile image by Hytec).

### -Hytec

The company Hytec (Montpellier, France) has developed a rotating laser, which performs exact measurement of the pipe's shape. It operates in pipelines of with 200 to 1000mm. The software for deflection calculation is included; the measured pipe profile can be viewed in real time on a PC color monitor. The VSLPC laser systems comes as integrated with a color TV camera.

### -Optimess

The company Optimess (Gera, Germany) offers the laser scanner OptiScan, originally developed by MFPA in Weimar, Germany [13]. The variant OptiScan200 (Fig. 2.7) operates in pipes from 200mm, at a measuring distance of 5-100cm and an accuracy of ± 1mm (according to vendor). Again, the software for calculating and visualizing the measured profile are available.
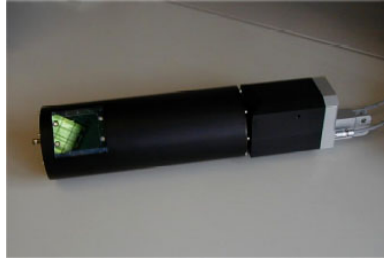
Figure 2.7: OptiScan

**Radar-like sensors**

Ground Penetrating Radar (GPR) systems are in general heavy and power consuming. The antenna systems are large with respect to the dimension of a pipe robot.

A first use of GPR with a sewer system was announced by the developers of the KARO. They developed a GPR small enough for a sewer system. They also used a micro wave device to inspect anomalies behind the pipe walls. They report that it is possible to distinguish from type of sources of different anomalies based on bubbles of air or water, pipe couplings and house connections.

Commercially available system are presented by Oyo and Burn Am. In the case of Oyo, no data in regard to the applicability of this tool is available (i.e. do the number and severity of hidden cavities balance the expense of the radar).

In contrast, Burn Am has developed the Ground Penetrating Radar Sensor to marketable stage. The present model is integrated to a tethered, remotely controlled platform, Fig. 2.8.



Figure 2.8: Ground penetrating radar by Burn Am.

**Chemical sensors**

An analysis of chemical and physical parameters in the sewage as well as in the atmosphere in sewers may yield information about corroding and poisonous substances in the sewage as well as damages in the pipe system (ground water leaking in). Sensors for measuring isolated basic parameters of that kind (temperature, acidity) are widely available. They can be made small. Their energy requirements are normally negligible. Their handling may be non-trivial for a fully autonomous robot, as sensors measuring in fluids (such as sensors for the acidity level) can function for short periods of time only, i.e., they need to be dipped actively into the sewage. We report here on some sensor prototypes aimed at sensing a wider range of chemicals.

### - "Nose on a chip"

The "nose on a chip", which could be incorporated into household gas appliances, consists of an array of tiny sensors on one integrated circuit and electronics on another. By selectively coating the micro cantilever arrays with appropriate chemicals, the chip can be customized to detect virtually any chemical or biological species. Developers say a single chip could detect thousands of chemicals.

### -KAMINA

KAMINA is a micro system for detecting and characterization of corrosive and process gas or smell in the atmosphere. The " Karlsruher Mikronase (Karlsruhe micro nose) " is constructed as a micro chip array made out of $SnO_2$, $WO_3$ a.o. based on measuring the electric conductivity of each array element. In a cycle once per second, gases like CO, $NO_2$, $NH_3$, $H_2S$ or organic gas and steam are detectable and quantifiable. The on-line evaluation is based on modern pattern recognition techniques and is customizable dependent on the purpose.

**More sensors for navigation and motion control**

Autonomous sewer robots must include sensors for their own control, navigation and localization, not only those for sewer state assessment and damage detection. These sensors may overlap with the inspection sensors (e.g., a camera may be used for both navigation and damage detection). Localization is an issue not only for the proper robot control, so that the robot knows where it is, but also for inspection, as detected damages have to be reported with their location. Sensors in this direction are available in great varieties,

and they are used as standard sensors in autonomous and semi-autonomous robots in other areas than sewer robotics. Note that sewer robots have the requirements in addition driver-less indoor transportation vehicles that their sensors be physically small and energy efficient.

### *-Compass*

For navigation purposes it is helpful to know the northern direction. Accordingly, a compass may be of help. Electronic compasses are widely available on the market. Note that compass readings may be noisy in a sewer robot due to the many objects of city infrastructure that can typically be found close to sewers (steel constructions, cables, etc.). Therefore, among available electronic compasses, only those should be used on a sewer robot that report possible disturbances of their readings.

### *-Inertial sensors*

- **Inclination sensors** Essential for helping to control tilt in fully autonomous or semiautonomous platforms. They are in use, e.g., in the KURT, MAKRO and KARO systems reported elsewhere in this thesis. They are widely available on the market, fitting the space and energy requirements of a sewer robot.

- **Accelerometers** Essential for helping the localization and control of fully autonomous robots.

- **Gyroscopes** Essential for measuring turns in autonomous robots. Widely available, but highly precise sensors are costly and may be large in build. All gyroscopes suffer from a systematical error of drift over time caused by the earth rotation.

## 2.5   Conventional inspection methods

Over the past ten years, Closed Circuit Television (CCTV) is the most commonly used internal sewer pipe inspection method. This method is carried out using a cable-tethered robot with an onboard video camera system. An operator remotely controls the movement of the robot and the video system (Fig. 2.9). By this video-supported visual inspection, any notable damages or abnormalities are recorded in video stream(Fig. 2.10). The reliability of this system depends on the experience of an operator.
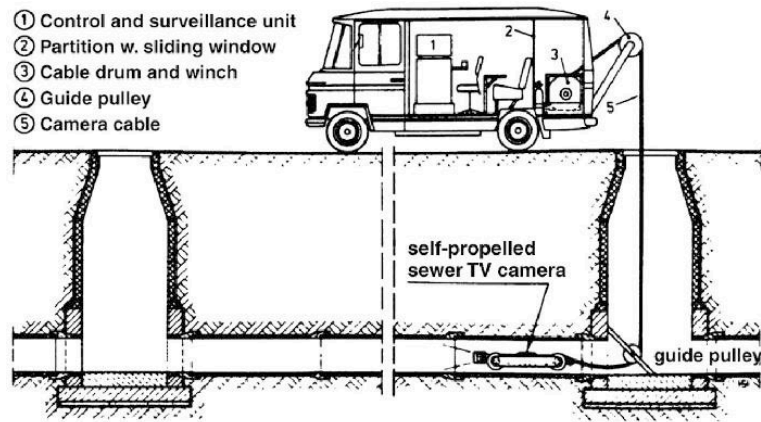
Figure 2.9: Diagram of visual inspection.



Figure 2.10: Operator with video monitor.

Recently, new and more accurate techniques have been fielded to conduct internal sewer pipe assessments. The methods used for inspecting pipe condition, fall into three broad categories:

- Inspection of inner pipe surface

- Inspection of pipe structure and bedding conditions

- Inspection of the pipe bedding

The first category, with which most practising engineers are most familiar, included CCTV (conventional, light line and computer assisted), laser scanning and ultrasound techniques. The second and third categories include micro deflection, impact echo and ground-penetrating techniques to assess the conditions of the pipe outer layer and surrounding soil. The cost and accuracy of these methods vary widely and some methods are only justified

15

in very specific situations where other methods will not produce an acceptable quality of information. Other inspection methods may be combined with CCTV inspection to verify the pipe condition assessment [14]. These methods may include soils testing, physical and chemical testing of removed pipe segments [15].

**Methods of inspecting the inner sewer wall surface**

*-CCTV inspection systems*

Standard pipe inspection systems are based on Closed Circuit Television (CCTV) cameras in a large range of application fields such as waste pipes and drains. The CCTV method consists of a mobile, remotelyoperated platform usually equipped with a colour, high-resolution video camera and a lighting system. The camera platform is connected via a multi-core cable to a remote inspection station with video recording facilities situated over ground. An engineer then assesses the recorded images off-line.

There are two basic types of the CCTV system. Each uses a television camera in conjunction with a video monitor, video cassette recorders and possibly other recording devices. In one case the inspection is performed using a stationary or zoom camera mounted at a manhole so that it looks into the sewer, while in the other a mobile, robotic system is placed within the sewer itself. Either form of CCTV inspection may miss certain types of defects, especially those that are hidden from the camera by obstructions as it looks down the sewer. Slight deformations of the sewer may go unnoticed, and any defects hidden beneath water inside the sewer will definitely not be found.

This is a subjective and time-consuming task that considerably increases the inspection costs. Moreover, only gross anomalies are evident to the human eye, which reduces the detection of faults at early stages. Another drawback associated with those systems in these particular environments is the lack of visibility inside the pipes and the poor quality of the acquired images that hinders a complete assessment of the pipe condition and sometimes even the detection of large defects.

*-Stationary CCTV systems*

Stationary video cameras mounted at a manhole are limited with respect to what they can see. Defects that are close to the manhole will be found, but the farther into the sewer a defect is, the harder it will be to identify and evaluate. Defects beyond the range of the camera would be missed entirely unless they cause secondary effects that can be identified at the manhole

(such as changes in water flow within the pipe between two manholes). One vendor of this technology suggests that the equipment be used as part of a screening process to determine which sewer sections should be completely examined by mobile CCTV systems. Stationary CCTV's usefulness in this respect will depend on whether the damage that can be detected by this type of system near a manhole in a sewer line is representative of that throughout the entire section of sewer line.

A survey of defects by IRC [16] indicates that, based on structural factors alone, stationary CCTV can readily be used to inspect vitrified clay sewers. In brick sewers the most efficient use of stationary CCTV would be to restrict it to inspecting sewer lines that are shorter than 50 metres in length, although a slightly greater factor of safety in the inspections would be produced by using the technique only on pipe sections that are less than 40 metres in length. While the results suggest that concrete pipes may be inspected in the same manner as vitrified clay pipes, too few concrete pipes were examined for a definitive conclusion to be reached.

### -Mobile CCTV systems

Mobile CCTV systems are the most common means of inspecting sewer lines.This type of CCTV system uses a camera mounted on a robot that enters the sewer system. The camera generally looks forward as the robot system moves along the sewer axis, allowing the operator to examine and evaluate the entire length between a pair of manholes. It is possible to modify this type of CCTV system to overcome many of the limitations of CCTV inspection discussed above. Some CCTV systems have" pan and tilt" cameras attached to the robot, which can find defects hidden from a forward looking camera behind connections and other obstructions within the sewer line. Sonar or ultrasound systems are often attached to robots to examine the sewer below the waterline. It is also possible to obtain CCTV equipment with a" light line" attachment to assist in quantifying smaller sewer deformations. This system projects a line of light around the circumference of the sewer being examined in order to assist in assessing the shape of the sewer.

### Inspecting within the pipe wall and the bedding condition

Although CCTV, laser and ultrasonic systems provide images of the inside surface of a pipe wall, they do not indicate what is happening within the pipe wall or behind it. While in some cases the observed damage to a pipe is due to internal problems such as erosion, in many others the damage is caused by external forces. The following inspection techniques allow the sewer owner

to examine the overall condition of an entire pipe wall, the soil behind a pipe or the pipe-soil system. Their ability to look beyond a pipe wall surface gives sewer owners opportunities to evaluate sewer condition in ways that are not possible with CCTV and similar techniques.

### -Wall micro-deflections and natural frequency of vibration

Measurements of wall micro-deflections and the natural frequencies of vibration of sewer lines are being developed specifically as a means of diagnosing brick sewer condition. The methods give information on the overall mechanical condition of the sewer line, rather than identifying specific defects.

A micro deflection in a pipe wall surface is created by applying pressure to the inside surface of the wall to very slightly deform it. In this case the intent is to measure the change in position versus the increase in pressure applied to the wall in order to indicate how well the grout between the bricks has been applied or whether the walls of a concrete or brick pipe have been damaged. It would be expected that a well grouted brick wall would expand continuously (although not equally) in all directions as the pressure increases, provided the pressure is below that which would damage the grouting. A similar, equal increase would be seen in an undamaged concrete or vitrified clay pipe.

Increasing in micro deflection in one direction while decreasing in another or a sudden change in the slope of a graph of applied force versus micro deflection would suggest that the wall was damaged. The major difficulty with this technique is determining the maximum safe pressure for use on a brick wall so that the inspection method does not damage it. This pressure will depend on the pre-existing condition of the sewer. While these pressures can be readily calculated for an undamaged sewer, the accuracy of such calculations is dependent on knowledge of the strength of the mortar or concrete at any given point in the sewer. This will vary depending on the age and condition of each sewer section. Care must therefore be taken to avoid damaging sewer sections that have below normal strength but are still able to function properly. This safety consideration is not as important for concrete pipes, where the strength of the pipe material is more uniform around the pipe circumference. Micro delfections are restricted in use to rigid pipes where an entire pipe wall will be deflected by the applied force. Plastics such as PVC and HDPE can not be inspected using this method as local deformation of the pipe wall would tend to provide a false indication of the pipe condition. The restriction of the technique to materials such as brick, concrete, metal and vitrified clay means that it is only sensitive to the wall condition, rather than that of the surrounding bedding. Measuring the

natural frequency of vibration also gives information about the mechanical behaviour of a pipe wall, but in this case the process involves vibrating the wall at a range of frequencies and determining which frequency gives the largest vibrations (the natural frequencies). A section of good wall would be expected to have certain characteristic natural frequencies, while deviations from those frequencies would indicate that the wall or surrounding bedding was deficient in some manner. The application of this technique depends on the development of an understanding of exactly how the natural frequencies of different types of pipe wall would be expected to change with increasing damage. However, other factors can also affect the results of the natural frequency measurement, including changes in bedding material or quality, the amount of water in the pipe and the height of ground water around the pipe. Considerable research is needed to determine if these effects can be separated from those produced by actual damage to the pipe wall.

### -Impact echo/spectral analysis of surface waves

These closely related techniques they have been successfully applied to the inspection of large, empty concrete pipes and large brick water lines. The SEKISUI Company has made a sewer inspection robot with a hammer and microphone. The apparatus consists of a source of controlled impacts, such as a falling weight or a large pneumatic hammer and one or more geo phones that are mounted against the wall of the pipeline. Low frequency surface waves are produced when the wall of the pipe is struck by the hammer or weight. These waves are then detected by the geo phones. The major difference between the two techniques is that impact echo generally looks only at the actual waveform produced by the impact, while spectral analysis of surface waves (SASW) uses more geo phones and separates the waves into different frequency components [17]. These different components travel at different speeds and penetrate to different depths in the soil beyond the pipe, allowing more information to be gathered about the condition of the pipe and surrounding soil.

Although the two techniques are similar, the use of the additional sensors and analysis in SASW means that it is possible to easily separate effects produced by soil conditions from those produced by problems in the pipe wall. SASW therefore is the most flexible of all the techniques discussed in this section since it is capable of investigating both pipe wall and soil condition at the same time. A drawback of Impact Echo and SASW inspection is that they are currently only available for manual use in large diameter tunnels that are easily accessible by human operators. Both techniques need to be automated to increase their inspection rate and allow deployment in smaller

diameter pipelines. A second drawback is that cleaning of the pipe walls is likely to be required before they can be used.

**Detecting conditions behind the pipe wall**

Although some of the inspection techniques described previously can give information about conditions behind a pipe wall, their primary use is likely to be in determining the structural soundness of the wall itself. By contrast, ground penetrating radar may occasionally give information about delaminations in concrete sewers, but its major use in sewer lines is in detected potential problems behind the sewer walls.

### -*Ground penetrating radar*

Ground Penetrating Radar (GPR) is a geophysical method that has been developed over the past thirty years for shallow, high-resolution, subsurface investigations of the earth. GPR uses high frequency pulsed electromagnetic waves (generally 10 MHz to 1,000 MHz) to acquire subsurface information. Energy is propagated downward into the ground and is reflected back to the surface from boundaries at which there are electrical property contrasts, Fig. 2.11 shows a diagram of the process. GPR is a method that is commonly used for environmental, engineering, archaeological, and other shallow investigations.
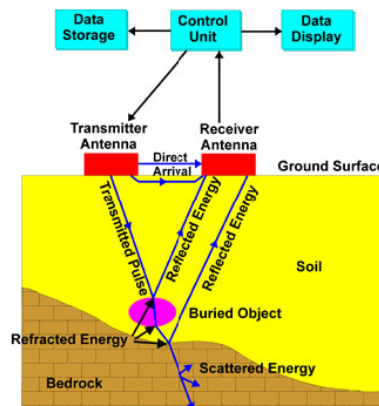


Figure 2.11: Ground penetrating radar schema.

Radar is well known for its ability to detect airplanes or other flying objects, but with significant adaptations it can also penetrate rocks, sand and other solid materials to detect buried objects and voids. GPR is widely used in locating lost utilities, environmental site characterization and monitoring,

agriculture, archaeological and forensic investigation, unexploded ordnance and land mine detection, groundwater, pavement and infrastructure characterization, mining, ice sounding, permafrost, void, cave and tunnel detection, sinkholes, subsidence, etc.It may be deployed from the surface by hand or vehicle. It has the highest resolution of any geophysical method for imaging the subsurface, with centimetre scale resolution sometimes possible.

Resolution is controlled by wavelength of the propagating electromagnetic wave in the ground. Resolution increases with increasing frequency (shorter wavelength). Depth of investigation varies from less than one meter in mineralogical clay soils like montmorillonite to more than 5,400 meters in polar ice. Depth of investigation increases with decreasing frequency but with decreasing resolution. Typical depths of investigation in fresh-water saturated, clay-free sands are about 30 meters. Depths of investigation (and resolution) are controlled by electrical properties through conduction losses, dielectric relaxation in water, electrochemical reactions at the mineralogical clay-water interface, scattering losses, and (rarely) magnetic relaxation losses in iron bearing minerals. Scattering losses are the result of spatial scales of heterogeneity approaching the size of the wavelength in the ground (like the difference between an ice cube and a snowball in scattering visible light).

The ability of GPR to detect subsurface voids has lead to an interest in using it to evaluate the condition of sewers and other pipes. While delaminations in concrete sewers could be detected by GPR systems, much of the interest in the technique is due to its ability to examine the bedding behind the pipe wall. Voids, rocks and regions of water saturation produced by exfiltration should all be readily detectable by the technique. Recent research on this application has investigated its use in brick sewers [18], transport tunnels and small diameter sewer lines [19].

Radar systems work by emitting a coherent beam of radio waves [20]. These waves travel through space, air or the ground until they reach an object with differing conductivity and dielectric constant, such as an airplane, a void in the ground or an area saturated with water. Part of the radar wave is reflected off the interface between the two objects and propagated back to the transmitter. The rest of the wave passes into the new object and continues to travel in the original direction. Radar beams can also be attenuated by the nature of the material through which they travel. Materials that are highly conductive, have high dielectric constants, or are magnetic will rapidly attenuate the radar beam. As a result radar is attenuated very rapidly in metals, giving essentially zero penetration, but can travel very long distances in air and space.

Sand, asphalt, clay and ice fall between these two extremes, with the degree of attenuation dependant on amount of liquid water and salts present in

the material. Ice is essentially transparent to GPR, allowing the technique to be used to map the bottoms of glaciers. It can also penetrate deeply in dry sand. However, the depth of penetration in wet sand is much less, and in clays the penetration is further reduced [21]. In these materials the presence of water increases the conductivity, while clays can also have significant dielectric constants. The presence of salt in the ground increases the soil conductivity and therefore further decreases the maximum penetration depth of a GPR system.

Radar can be used to locate leaks in buried water pipes either by detecting voids in the soil created by leaking water as it circulates near the pipe, or by detecting segments of pipe which appear deeper than they are because of the increase in the dielectric constant of adjacent soil saturated by leaking water. Ground penetrating radar waves are partially reflected back to the ground surface when they encounter an anomaly in dielectric properties, for example, a void or pipe. An image of the size and shape of the object is formed by radar time-traces obtained by scanning the ground surface. The time lag between transmitted and reflected radar waves determines the depth of the reflecting object.

In sewer pipes application, a radar antenna moves inside the sewer and is cable connected to a recording unit above ground. GPR may be used to detect water leaks in two ways:

- Identifying soil cavities created by the turbulent flow of leaking water.

- Identifying pipe segments, which appear deeper than expected because of the increase of the dielectric constant of adjacent soil, saturated by leaking water.

Despite a number of problems GPR has been employed in the condition assessment process for sewer lines in France since the early eighties. Data inspection requires substantial experience and training because the radar output is very difficult to interpret.

These techniques may be used from either the ground surface or from within the pipe but does not provide specific information on the pipe wall condition. For above ground use the technique is used to either identify the presence of pipe segments or the presence of voids surrounding the pipe, both by measuring the changing dielectric of the soil, cavities and pipes. For within pipe use the technique is used to identify cavities in the soil behind the pipe wall. In traditional above ground penetrating radar techniques, both transmitting and recording devices are mounted on the ground surface above the pipe.

## 2.6 Difficulties in conventional systems

The conventional inspection systems used for inspecting pipe condition in three broad categories are described in section 2.5. Among them, we focus on inspection of inner pipe surface and discuss about the difficulties in covential systems.

Each of the systems for inspecting the inner surface of the pipe wall provides similar types of information to the manager of a sewer system. Conventional CCTV's long history of use means that new systems inspecting the same area must provide substantial advantages in the quality of information provided or in lower costs before they will be adopted for common use. Table 2.4 summarises the advantages and disadvantages of each inspection methods.

The described modifications to conventional CCTV can assist in interpreting the results of a CCTV inspection, but are unlikely to be widely adopted unless their cost is not significantly higher than that of conventional CCTV alone. Stationary CCTV cameras are therefore the most likely application to enter common use, as they offer the opportunity to do preliminary examinations of the shorter pipes in a city's sewer system without cleaning. Mobile CCTV systems offer noticeable advantages in identifying the presence of deformation, but are essentially an evolutionary enhancement of the standard CCTV system, rather than a revolutionary improvement.

## 2.7 Autonomous sewer robot platform, KAN-TARO

The sewer system, which is inherently narrow, slippery, and dirty and wet, is not an easy place for a robot. A robot is supposed to move through long pipes quickly with minimum consumption of energy, and to turn at narrow and slippery junctions with minimum mechanical wear. Due to remaining water in sewer system during inspection, the robot must be waterproof. Taking these requirements into account, we design a novel mechanism satisfying all the requirements.

The conventional sewer robots are able to move through straight pipes, but unable to smoothly turn at junctions. Robots capable of smooth turning at junctions are desired.

We design novel and compact moving mechanism, KANTARO(Fig. 2.12) for sewer pipe inspection robots based on passive adaptation of wheels to the bends of pipes [66, 68, 72]. This is accomplished by proper wheel orientation and passive damping of springs. A robot with this new moving mechanism

Table 2.4: Summarises the advantages and disadvantages of conventional inspection methods.

| Methods | |
|---|---|
| CCTV inspection systems | Advantage<br>- standard technique.<br>- considerable body of knowledge.<br>- available to aid in interpreting results.<br>- relatively cheap.<br>- evaluates the entire length of sewer.<br><br>Disadvantage<br>- substantial operator interpretation of results.<br>- difficult to accurately compare two evaluations of the same sewer conducted at different times.<br>- may miss defects hidden behind obstructions or under water. |
| Stationary CCTV systems | Advantage<br>- cheaper than CCTV.<br>- possibly useful as a screening mechanism for other techniques.<br><br>Disadvantage<br>in addition to those listed for CCTV;<br>- only examines the sewer near manholes.<br>- long brick sewers are likely to be incorrectly.<br>- classified as undamaged. |
| Mobile CCTV systems | Advantage<br>As for conventional CCTV except;<br>- better estimation of sewer deformation.<br><br>Disadvantage<br>As for conventional CCTV except;<br>-greater expense than conventional CCTV. |
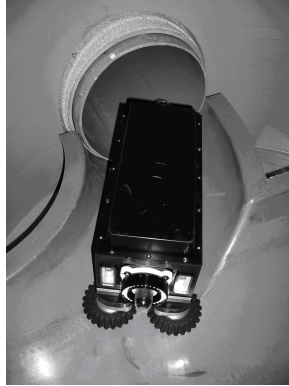
Figure 2.12: An autonomous sewer robot platform, KANTARO.

is able to carry a controller, electronics, motors and sensors, and to move through any bends of the pipes, to move through different sized pipes, to step down, and to pass obstacles without sensors and intelligent control.

To realize less wiring and easy assembling/disassembling of a robot, KAN-TARO designed as a modular type robot. Fig. 2.13 illustrates the robot consisting of two parts, i.e., the upper box and the lower box, connected to each other by the main connector.
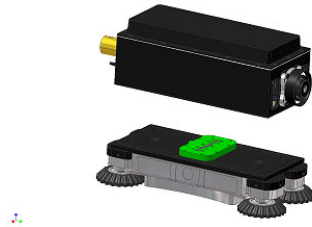


Figure 2.13: The KANTARO mechanism.

Sewer inspection is done while the water level in the pipe is low. Still, we need a robot waterproofed to prevent sensitive boards and sensors from damage. To satisfy this requirement, KANTARO's upper box and lower box are waterproofed.

# Chapter 3

# A vision-based automated fault detection system

## 3.1 Introduction

Automation is an important issue in industry, particularly in inspection works of underground facilities. This section describes an intelligent system for automatically detecting faulty areas in a sewer pipe system based on images. The proposed system can detect various types of faults and be implemented in a real time system. The present paper describes system architecture and focuses on two modules of image preprocessing and detection of faulty areas. The proposed approach demonstrates high performance in detection and reduction of time and cost.

Pipe walls in sewer systems are prone to be damaged due to aging, traffic and chemical reactions, through which inflow such as rainwater and groundwater seeps into pipe systems. Regional city government reports [22] state that this inflow amounts to approximately 30% of the total flow. In addition to the inflow of groundwater into sewer pipes, outflow from damaged systems also occurs, contaminating the surrounding environment [23]-[25].

Basically, maintenance or inspection process starts by collecting information about the utility. It highlights useful information about conditions of the utility such as the number and the location of faults.

Conventional inspection of a sewer pipe system is carried out using a cable-tethered robot with an onboard video camera system. An operator remotely controls the movement of the robot and the video system (Fig. 2.9). By this video-supported visual inspection, any notable damages or abnormalities are recorded in video stream. The reliability of this system depends on the experience of an operator. The system is also prone to human

error, and tends to be time consuming and expensive. Consequently, effective automated online techniques to identify and extract objects of interest such as cracks are of immediate concern.

Most previous works[26] focused on specific types of faults in sewer pipes such as displaced joints and surface cracks. Carino [27] gives a detailed overview of crack detection strategies such as infrared thermography, stress wave propagation methods and a ground-penetrating radar. Many detection strategies are developed assuming specific pipe materials. Since widely used materials such as concrete and clay have heterogeneous compositions, it makes applications of simple fault detection methods problematic.

Widely used techniques for steel pipes such as the one by Stavroulakis et al.[28] are not applicable to PVC or concrete pipes due to their nonconducting characteristics. Given feature detection methods with appropriate sophistication and sensitivity, low cost and general-purpose systems such as video cameras can play an important role in fault detection of sewer pipes.

Robust detection of cracks and other faults in sewer pipes based on sensory data is an important challenge. Bernatzki et al. [29] introduced a method for detecting small cracks in oil and gas pipelines. Raw ultrasonic data were transformed to time-frequency representation by the wavelet transform. Edges were detected by the real part of wavelet coefficients. Artificial neural networks were also used for classification.

Yoshimura et al. [30] described applications of an inverse analysis method based on neural networks and a finite element method to the identification of cracks in solid objects using laser and ultrasonic sensors. They used Error Propagation Coefficients to evaluate the accuracy of a neuro-based method for crack identification. They are able to identify surface defect with a detection error rate of 2.4%-12.0%, and the depths with an accuracy of 0.6%-4.1%.

For high dimensional spatially distributed data, wavelets may provide useful feature detection. Mojsilovic et al.[31] used Haar wavelets for decomposition and classification of myocardial tissue images. Gunatilake et al. [32] introduced a mobile robot platform that provided images in real time for remote aircraft surface inspection. A widely practiced crack detection algorithm is applied under directional lighting. It is a two-step multi-resolution edge detection method: a region of interest (ROI) is first converted into those with multiple resolutions by successive smoothing, followed by edge detection at each resolution. Wavelet-based filters are used for the conversion of ROI into those with multiple resolutions and for estimation of intensity variation for multi-resolution edge detection.

All above previous works focused on specific types of faults in pipes and none of them propose a method for detecting various types of faults. Accordingly, an automated fault detection system is not available in the real

world. We propose a method for detecting faulty areas based on images, and proposes an automated intelligent system designed to facilitate diagnosis of faulty areas in a sewer pipes system. The system utilizes image analysis and efficient techniques for providing the location and the number of faults in a sewer pipe system [74, 78].

## 3.2    Types of faults in the sewer pipe system

Japan Sewage Works Association (JSWA)[33] classfied three ranks (A,B and C) for various faults in sewer pipe system. Most visible faults defined as rank A, visible faults as rank B and hardly visible faults as rank C (see Fig. 3.1). Table 3.1 shows the differents faults classifications.



Rank A            Rank B            Rank C
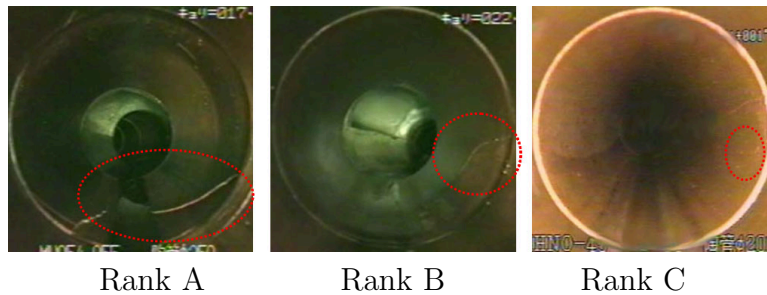
Figure 3.1: An example of differents ranks of crack.

Also, JSWA defined the corresponding task to be done for each rank in Table 3.2.

Based on the above table, we can say, the automated system which is able to detect the faults in rank A and B is acceptable for sewer pipe inspection.

## 3.3    Proposed system

As we mentioned in Introduction, in the conventional inspection systems, any notable damages or abnormalities in sewer pipe are detected by human. This system, therefore, is prone to human error, and tends to be time consuming and expensive. To overcome this difficulty, we propose an automated intelligent fault detection system. An overview of the proposed system is shown in Fig. 3.2.

Digital images of sewer pipes taken by the camera system on the inspection robot are given to the fault detection system. The system, then, extracts a ring ROI image to which edge enhancement is applied as preprocessing.

Table 3.1: The differents faults classifications.

| Category | A rank | B rank | C rank |
|---|---|---|---|
| Crack | The width of crack is more than 5mm in circumference direction | The width of crack is more than 2mm in circumference direction | The width of crack is up to 2mm in circumference direction |
| Water infiltration | Blown out | Flown out | Exuded |
| Root invasion | Invade more than 50% of pipe | Invade less than 50% of pipe | Invade less than 20% of pipe |
| Pipe break | Heavy damage | Having cracks entirely | Crack detection other than rank B |
| Joint and gap | Coming off entirely | Coming off partially | small gap |
| Mounting pipe projection | Project more than 50% of the diameter of the pipe | Project between 25% and 50% of the diameter of the pipe | Project less than 25% of the diameter of the pipe |
| Adhesion of mortar | Covered more than 30% of the diameter of the pipe | Covered between 10 and 30% of the diameter of the pipe | Covered less than 10% of the diameter of the pipe |
| Foreign substance | Blocked up by other than filth | Mixed with obstacle and others | An obstacle itself such as a cement bag |
| Adhesion of grease | Block up more than 50% of the diameter of the pipe | Block up less than 50% of the diameter of the pipe | Block up less than 20% of the diameter of the pipe |

Table 3.2: Corresponding task to be done for each rank.

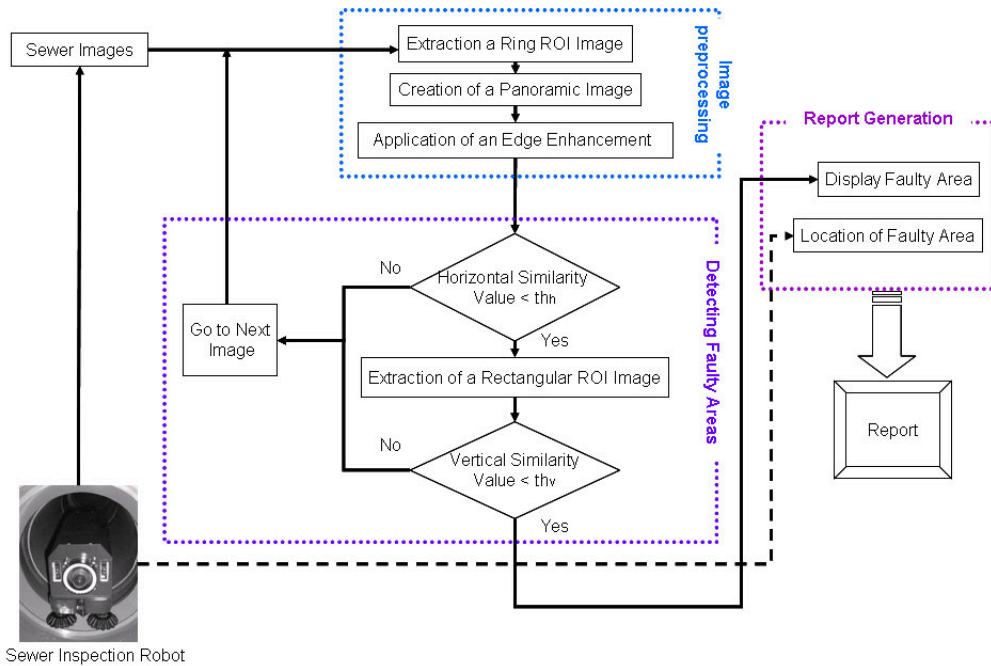| Levels | The inspection result | Corresponding task to be done |
|---|---|---|
| 1 | too much rank A faults | repair immediately |
| 2 | too much rank B faults + a few rank A faults | by a simple maintenance, repairing can be extend by 5 years |
| 3 | too much rank C faults + a few rank B faults + no rank A faults | by a simple maintenance, repairing can be extend more than 5 years |

Figure 3.2: An overview of the automated intelligent fault detection system.

Next, a newly defined measure of similarity is computed in order to extract candidates for visible faulty area in the ring ROI areas. Conjecture here is that the measure of similarity between images without faulty area is large. Hence, we focus on the area where the similarity value is smaller than a horizontal threshold, $th_h$, ranged between 0 and 1. The horizontal threshold is a value between 0 to 1 and change of this value directly effect to the number of detected faulty images in this step. Next, we extract a rectangular ROI and compute the autocorrelation value in the candidate faulty areas. Here, the area with autocorrelation value smaller than a vertical threshold, $th_v$, is defined as a faulty area. The proposed approach can detect even faint faults in this rectangular ROI area. The fault detection module demonstrates high detection performance based on the similarity in ring ROI and rectangular ROI areas. Finally the detected faults and its locations are compiled as a report. Here the location information on faults is provided by sensors on the robot such as an encorder, IR and a laser scanner.

**Image preprocessing**

At this step, the system first extracts ring ROI images. The panoramic image from the extracted ring ROI image is created by converting the luminosity of

30

each pixel at $(x, y)$ into that at $(r, \theta)$ in the panoramic image (Fig. 3.3). The relation between them is;

$$x = r \cos \theta, y = r \sin \theta \qquad (3.1)$$
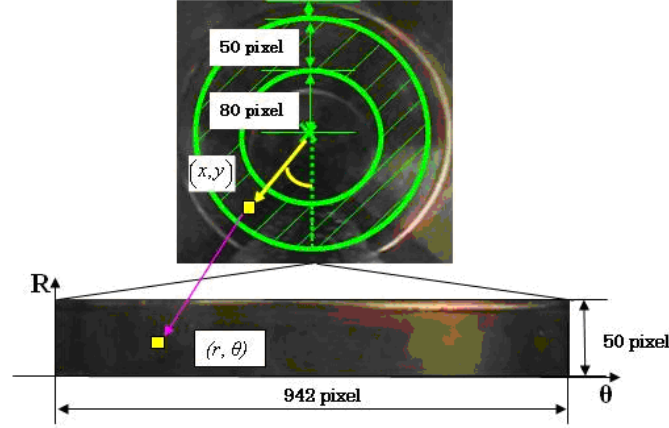


Figure 3.3: Extraction of the ring ROI.

Because of the variation of brightness in a faulty area in sewer pipes, edge enhancement in the following steps is applied to the panoramic image.

1. Convert the RGB into the brightness (Y).

$$Y = 0.3 \times R + 0.6 \times G + 0.1 \times B \qquad (3.2)$$

2. Use a Gaussian filter to reduce noise.

3. Detect edges. There are many methods for edge detection. Most of them are grouped into two categories: Gradient and Laplacian. In this paper, we use the Sobel and Prewitt gradient operators, and the Laplacian operator.

**Detecting faulty areas**

In the last step, the panoramic image (width=942 pixel, height=50 pixel) is created from the extracted ring ROI image. We define an average image of the panoramic image with the width, $w_1 = 50$ pixel, and the height, $h_1 = 50$ pixel. Then, we use a measure of similarity between the average image and panoramic image (Fig. 3.4) by the following equation.
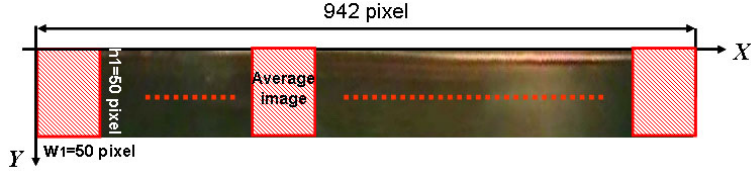
Figure 3.4: Horizontal similarity computation.

Suppose we have a set of images without fault. A conjecture here is that the measure of similarity between images without faulty area is large. Hence, the area with small similarity than a horizontal threshold, $th_h$, can be detected as a candidate faulty area.

$$C(x) = \frac{1}{w_1 \times h_1 \times 255} \sum_{i=1}^{w_1} \sum_{j=1}^{h_1} (255 - |I(i+x,j) - \bar{I}(i,j)|)$$

$$\bar{I}(i,j) = \frac{1}{N_1} \sum_{k=1}^{N_1} I(i+k,j) \qquad x = (0, 25, ......, 875) \qquad (3.3)$$

where $I(i,j)$ is the brightness of the pixel at $(i,j)$, and $x$ is the pixel coordinate in the horizontal axis in the panoramic image. $\bar{I}$ is the average of brightness at the average image and $N_1$ is the number of images used for creating the average image and defined as follows;

$$N_1 = width \quad of \quad panoramic \quad image - w_1 = 942 - w_1 \qquad (3.4)$$

Then, we focus on the candidate faulty area. We extract a rectangular ROI and compute the similarity value in vertical direction (Fig.3.5) to improve the detection rate based on the following equation.



Figure 3.5: Vertical similarity computation.

$$C(y) = \frac{1}{w_2 \times h_2 \times 255} \sum_{m=0}^{8} \sum_{i=0}^{w_2} \sum_{j=0}^{h_2} (255 - |I(i, j + y) - I(i, j + 5m)|)$$

$$y = (0, 5, ......., 40) \quad (3.5)$$
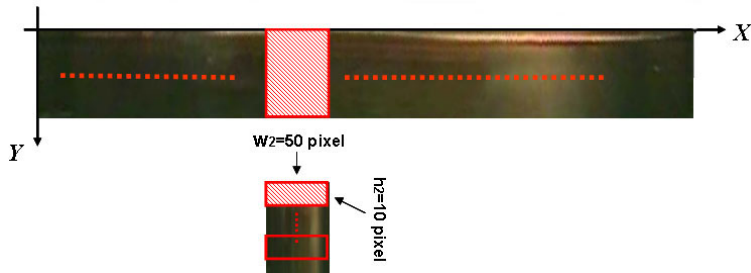
where $w_2 = 50$ pixel, $h_2 = 10$ pixel and $N_2 = 50 - h_2$. Finally, the area with similarity smaller than a vertical threshold, $th_v$, is detected as a faulty area. The proposed approach can detect even faint faulty areas in this rectangular area.

## 3.4    Experimental results

We evaluate the proposed method for detection of faulty areas using 253 images with 9 types of faults in Table 3.3 provided by a sewer inspection company. The image size is $640 \times 480$ pixel.

Table 3.3: The number of categorized images used for evaluation.

| Category | The number of images | A rank images | B rank images | C rank images |
|---|---|---|---|---|
| crack | 34 | 23 | 7 | 4 |
| water infiltration | 6 | 4 | 1 | 1 |
| root invasion | 25 | 17 | 6 | 2 |
| pipe break | 27 | 23 | 3 | 1 |
| joint and gap | 16 | 10 | 4 | 2 |
| mounting pipe projection | 8 | 5 | 1 | 2 |
| adhesion of mortar | 13 | 9 | 2 | 2 |
| foreign substance | 11 | 7 | 3 | 1 |
| adhesion of grease | 7 | 4 | 2 | 1 |
| Non-Faulty Image | 106 | | | |
| Total | 253 | | | |

We use 3 types of edge detection operators, Sobel, Prewitt and Laplacian, for comparison of the ability of detection in ring ROI area. Here,"true positive" is defined as the ratio of the number of correctly detected faulty images to the total number of faulty images. Similarly, "false positive" is defined as the ratio of the number of non-faulty images classified as faulty to the total number of non-faulty images. Fig. 3.6 illustrates false positive versus true

positive for different edge detection operators when horizontal threshold is changed from 0.8 to 1 by increment of 0.1. In ring ROI areas, the Sobel and Prewitt operators show almost the same performance, and is superior to the Laplacian operator.
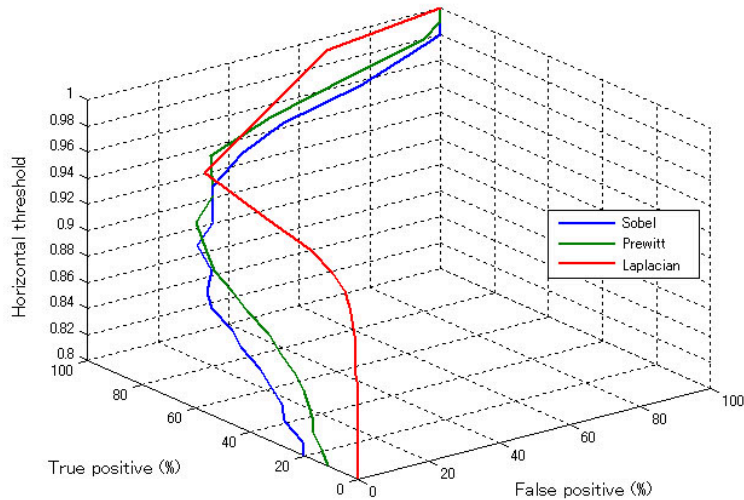


Figure 3.6: Performance of detection in the ring ROI area for different edge detection operators when horizontal threshold is changed from 0.8 to 1 by increment of 0.1.

Fig. 3.7 illustrates examples of detection of faulty areas by the Sobel operator in ring ROI areas. Figs. 3.7(b) and (d) show the successfully detected cases, marking the faulty areas with green circles. Failure sometimes occurs due to the false positive rate of 50% in ring ROI area. (Fig. 3.7(f))

As in the traditional statistical test, we aim at maximizing the true positive rate, keeping the false positive rate at a predetermined level called the level of significance.

To achieve high detection rate, we choose a high horizontal threshold value in the similarity computation to detect a wide variety of faults in ring ROI. Computation of the autocorrelation value in rectangular ROI area enables detection of even faint faults. Fig. 3.8 illustrates examples of detection of faint faults in rectangular ROI area.

Fig. 3.9 shows the performance of detection in rectangular ROI areas using Sobel operator for four different horizontal thresholds when vertical threshold is changed from 0.8 to 1 by increment of 0.1. Horizontal threshold value of 0.97 provides good performance.

34
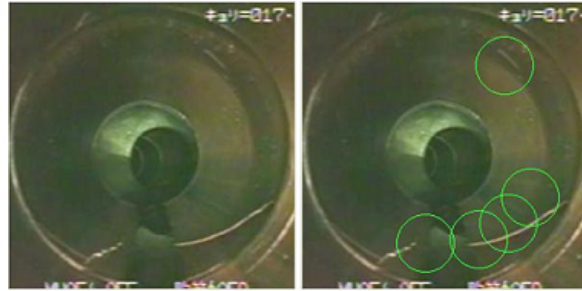
(a)The sewer image with the crack (b)The detected crack (successful)
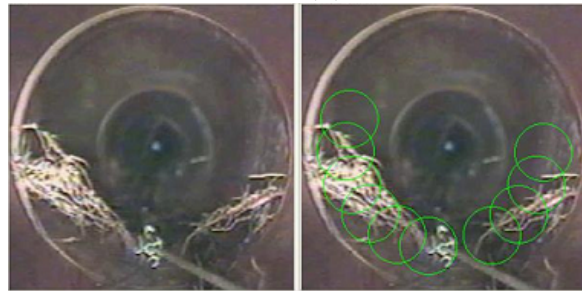


(c)The sewer image with the root invasion (d)The detected root (successful)



(e)The sewer image with the crack (f)The detected crack (failure)

Figure 3.7: Examples of detecting faulty areas in ring ROI area by proposed method.



(a)The sewer image with the crack (b)The detected crack (successful)

Figure 3.8: Examples of detecting faint faulty areas in rectangular ROI area by proposed method.
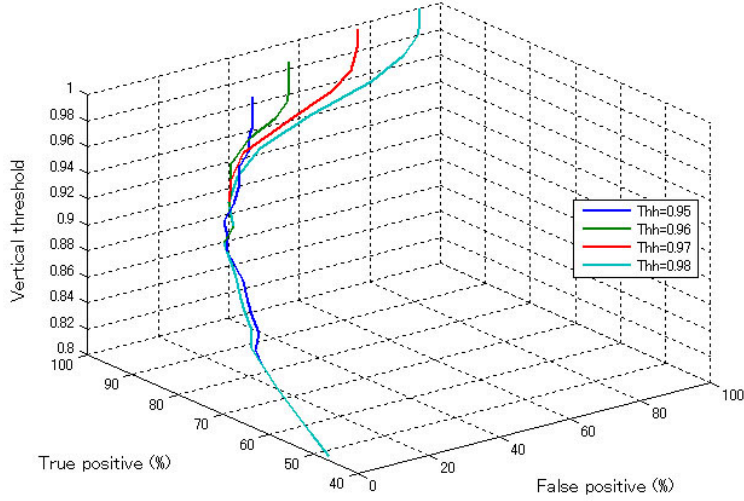
Figure 3.9: Performance of detection in rectangular ROI areas using Sobel operator for four different horizontal thresholds when vertical threshold is changed from 0.8 to 1 by increment of 0.1.
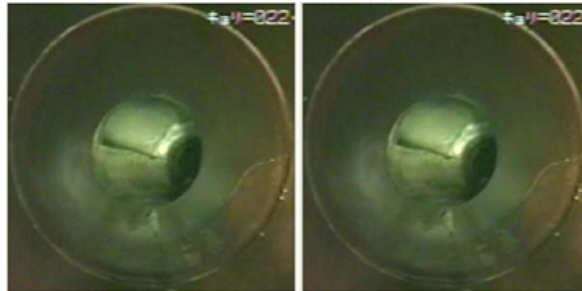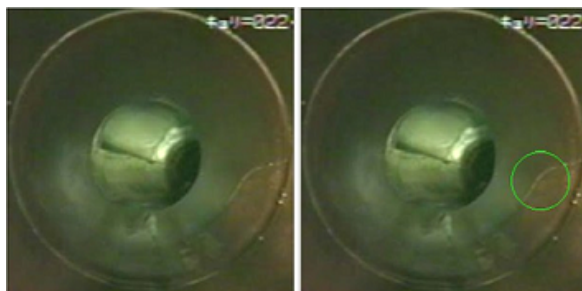
Next, we focus on different ranks when horizontal thresholds is set to 0.97 and vertical threshold is changed from 0.8 to 1 by increment of 0.1. The performance of this evaluation is shown in Fig. 3.10. When the false positive rate is 34%, the true positive rate is 100% for rank A and B, and 98% for rank C. The vertical threshold at this point is 0.96.

As we mentioned in section 3.2, the automated system which is able to detect the rank A and B faults is acceptable for sewer pipe inspection. Supposing the false positive rate of 34%, we can attain the true positive rate of 100% by the proposed algorithm for the sewer pipe images. We also showed this results to Water Environmental Section in Kitakyushu City, and they also confirmed 100% detection with 34% false positive rate is acceptable, and we can say that the proposed method succeeds in attaining 100% true positive rate and in the reduction of time and cost in sewer inspection.

## 3.5 Conclusions and discussions

We have proposed an intelligent system for detecting faulty areas automatically and implemented it in a real time system to solve the "real-world" problems in civil robots. In contrast to the conventional manual system, the proposed system can automatically detect faults and run in real time. It's

36
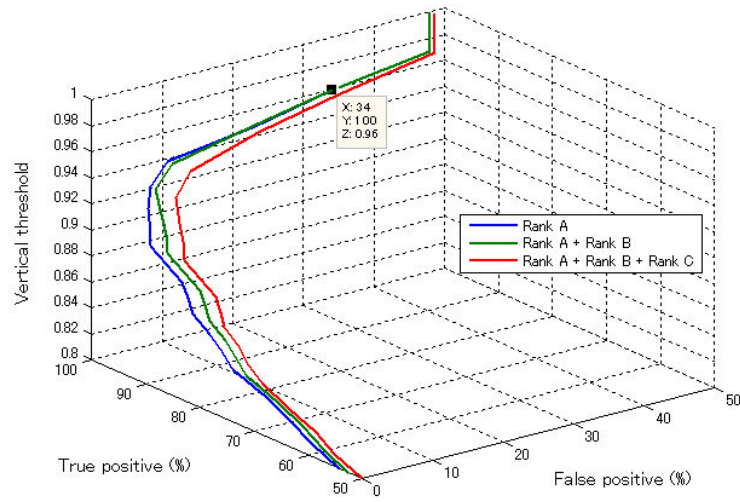
Figure 3.10: Performance of proposed method for different ranks when horizontal thresholds is set to 0.97 and vertical threshold is changed from 0.8 to 1 by increment of 0.1.

detection performance is 100%, when the false positive rate is 34%. This ratio is acceptable for sewer inspection, and the reduction of time and cost are also realized.

Future work should aim at further decrease in the false positive rate by keeping high true positive and to find other superior techniques for fault detection.

# Chapter 4

# Navigation based on single camera and IR sensors

## 4.1 Introduction

One of the central issues in developing an autonomous sewer robot is its navigation. Detecting landmarks such as manholes, inlets and joints in a sewer pipe system is an important task in navigation.

Various methods have been proposed for the detection of landmarks. Hertzberg and Kirchner conducted experiments on navigation of a sewer robot in a dry sewer test field at GMD, Sankt Augustin [34]. They succeeded in detecting local features by ultrasonic sensors. The detected landmarks were then scanned by a different, pivoted ultrasonic transducer. Finally, local features obtained by the scanner are classified using a specially trained artificial neural network. Although this method has a high rate of classification (75 out of 81 samples), it lacks the capability of locating an individual manhole.

Schonherr et al. [35] proposed a pivoted ultrasonic transducer that permanently scans the walls of the upper half section of pipes for detecting inlet. This procedure is time consuming. Paletta et al. proposed a method for detecting inlets from grayscale images taken by an onboard CCD camera [36]. Although it involves a time consuming training phase, the detection of inlets by trained neural networks is fast.

In a real sewer pipe system, a robot is required to explore unknown sewer area during the training phase. This property of time consuming training is undesirable from a practical point of view. To automatically detect damages in sewer pipes, Campbell et al.[37] and Clarke[38] proposed pipe profiling methods for 3D reconstruction. Using sensor devices mounted on a teleop-
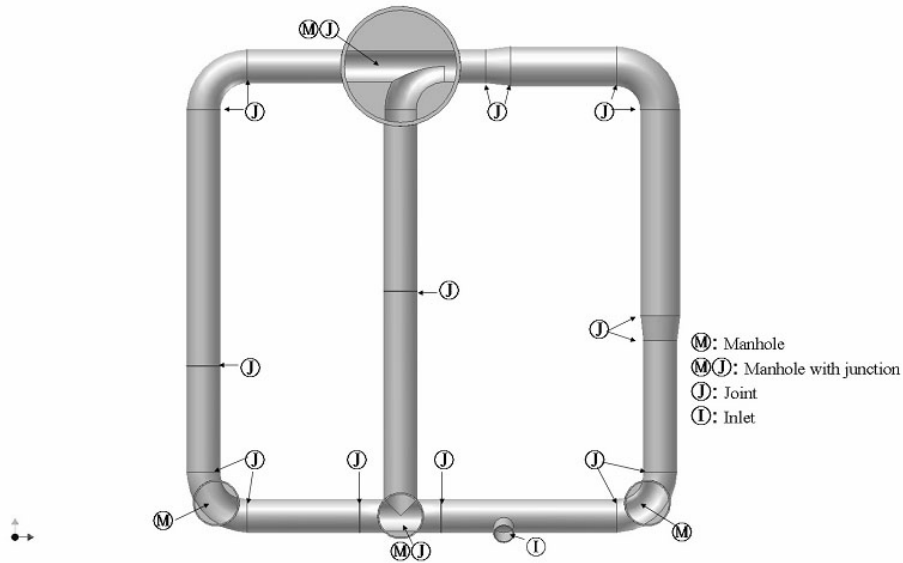
Figure 4.1: Landmarks in the sewer pipe system.

erated sewer robot, data evaluation is performed in a stationary surveillance vehicle.

Our method is capable of self localization and landmark detection by using an IR and single camera sensors [69]. In our method, the images are captured by a CCD camera at the front of a robot. The distance between robot and landmarks are estimated based on image data. The exact locations of the landmarks are compute by IR sensor data. Finally, information on the locations of a robot and landmarks are used for fault localization and robot navigation.

## 4.2 Landmarks in sewer pipe system

Ordinary in sewer pipe systems, any changing in the direction of pipe or any intersection between three or more pipes is called pipe-bend. In according the rule of sewer pipe construction, there is a manhole over each pipe-bend. Pipe-bends in sewer pipe system can be classified in three main types depend on their construction and shape; Curves, Joints, T-Junctions. Fig. 4.1 illustrates the sewer pipe construction with the manhole over each pipe-bend, inlets from houses, and joints connecting two pipes.

For navigation in a sewer pipe system, a robot needs distinctive landmarks. Elements like manholes, junctions, inlets and pipe joints are well suited for this purpose. As shown in Fig. 4.2, manholes are always located

(a)Manhole        (b)Joint        (c)Inlet

Figure 4.2: Location of the landmarks in the sewer images.

in the upper part of the sewer image, while joints and inlets are always in the central and upper half of the sewer image. This makes easy the extraction of their positions from the image. The fact that the maximum length of a plastic or ceramic pipe is less than 2m makes cap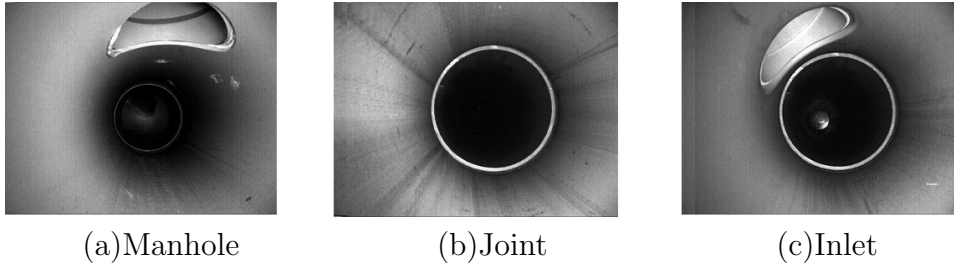turing landmarks still easier. The resulting map has descriptions on manholes, inlets, pipe joints, the distance between them and so forth.

## 4.3 Methodology

Autonomous sewer robots must include sensors for their own control, navigation and localization, not only those for sewer state assessment and damage detection. These sensors may overlap with the inspection sensors (e.g., a camera may be used for both navigation and fault detection). Localization is an issue not only for the proper robot control, so that the robot knows where it is, but also for inspection, as detected faults have to be reported with their location.

We propose a method to cover self localization and landmarks detection for an autonomous robot by fusing of IR and camera sensors data. As we mention in 4.2, four landmarks are exist in sewer pipe systems and the robot may stop or changing its moving direction in two of them, manholes or junctions. Therefore we involved IR sensor to detect this two landmarks approximately. Fig.4.3 illustrates the overview of the proposed method. First a sewer pipe image is provided to the system and four ROI images are extracting. By computing the self localization, the distance between robot and landmarks will estimate and if this distance value is less than 10cm, the system check the IR sensors value. Here if the sensor value is less than a threshold then the exact location of two landmarks will detect.
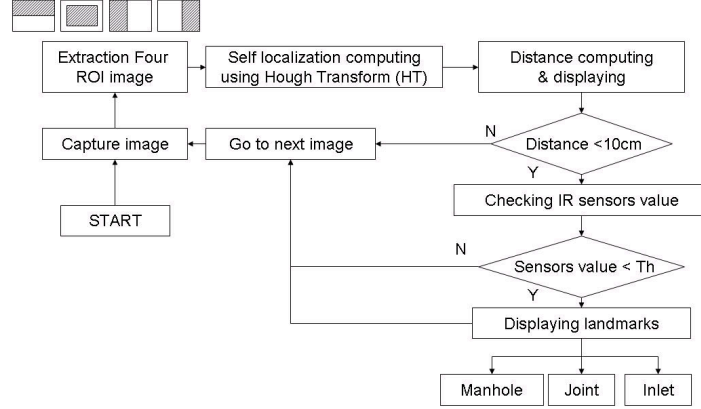
Figure 4.3: Overview of the proposed method.

## Computation of self localization

In this step, we use Hough Transform (HT) for self localization computing. The Hough transform is a feature extraction technique used in digital image processing. The classical transform identifies lines in the image, but it has been extended to identifying positions of arbitrary shapes such as circle and curve. The underlying principle of the hough transform is that there are an infinite number of potential lines that pass through any point, each at a different orientation. The purpose of the transform is to determine which of these theoretical lines pass through most features in an image, that is, which lines fit most closely to the data in the image.

In our case, the hough transform is used for extracting of circles, the shapes of landmarks in sewer images. A circle in the image space can be described by, $(x_i - a)^2 + (y_i - b)^2 = r^2$, where $(x_i, y_i)$ is the poin on the circumference of circle. An infinite number of circle is possible to pass through any point on the circumference, with differents center $(a, b)$ and radius $r$ (Fig. 4.4). $(a, b, r)$ are three parameters which span a 3D hough space (Parameter space).

Any point $(x_i, y_i)$ in the image space corresponds to a cone shaped surface in the 3D parameter space. Each point in the cone is said to vote for a set of bins corresponding to the circles that pass through it. By finding the bins with the highest value, the most likely circles can be extracted, and their geometric definitions read off.

In details, four ROI images will extract from input images. Then, The cany edge operator is applied to input images for edge detection in each ROI

41
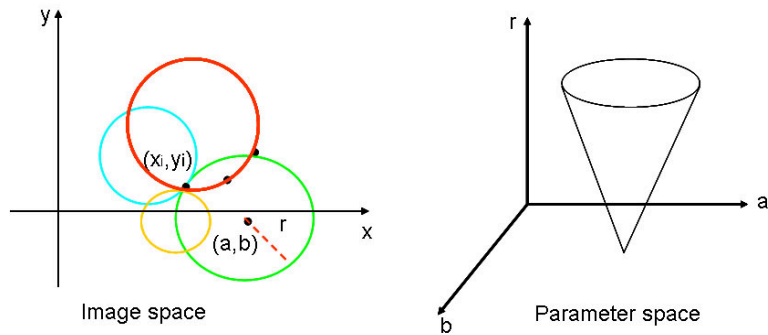
Figure 4.4: Hough transform for circle.
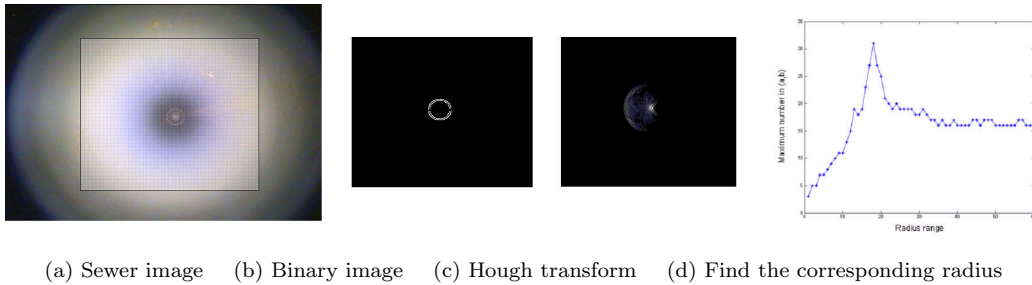


(a) Sewer image    (b) Binary image    (c) Hough transform    (d) Find the corresponding radius

Figure 4.5: An example of self localization computing with pipe joint image.

images and convert to binary images. Next, we define 3D hough matrix with 3 unknown parameter, $(a, b, r)$. To help for fast computing, we reserve the range of r in hough matrix. The hough transform will perform and the local maximum value in $(a, b)$ will indicate the correspond $r$ for the circle. Finally, we estimate the distance between the robot and landmarks based on compared each circle radius with corresponding radius-distance data in field test by KANTARO. Fig. 4.5 show an example of self localization computing with pipe joint image.

**Detection of landmarks by an IR sensor**

Self localization computing based on image data still has some error, hence the IR sensors data are applied to detect manholes and junctions exact location. These two landmarks must be executed with high precision, because misperception such as early turning action in junctions causes damage to robot, so, we involved three IR sensors as shown in fig.4.6. Fig.4.7 and Fig. 4.8 verified the IR sensor values shows a large variation when the robot is at one of these two landmarks.
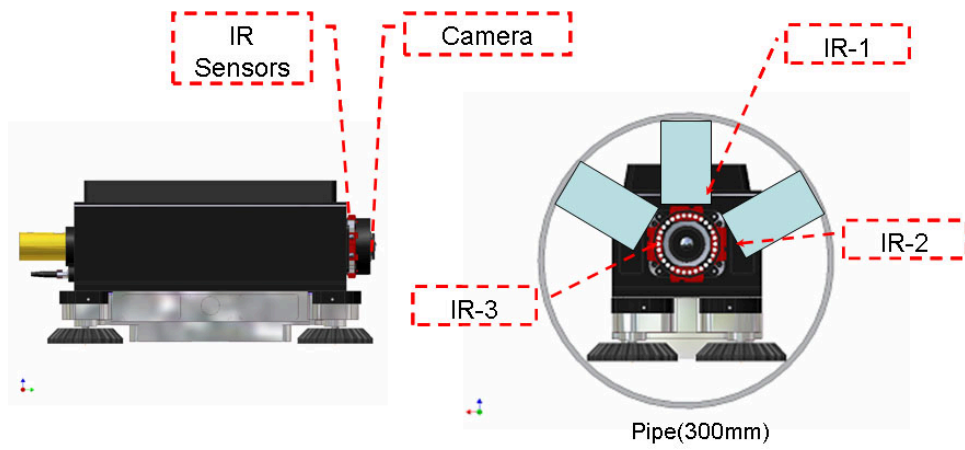
Figure 4.6: Position of IR sensors and camera.
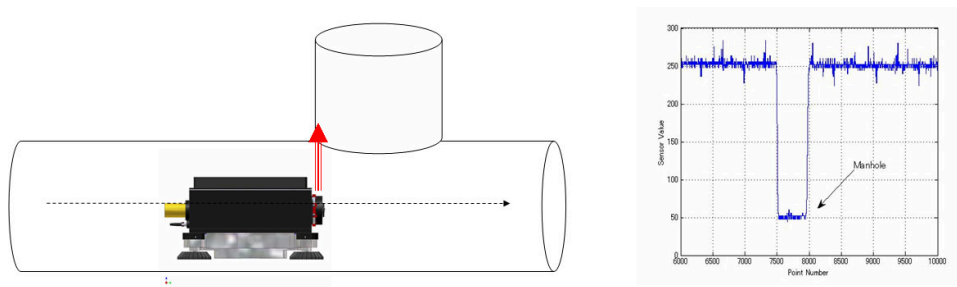


Figure 4.7: IR-1 sensor value when the robot is at the manhole.
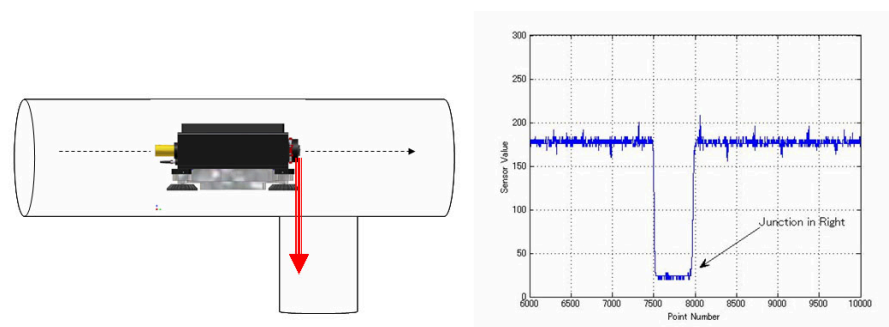


Figure 4.8: IR-3 sensor value when the robot is at the junction.

43

## 4.4 Experimental results



Figure 4.9: Dry sewer test field at the FAIS-RDSO.

Images of KANTARO moving through the pipe are acquired in the dry sewer test field at the FAIS-RDSO in Fig.4.9. The dry sewer test field is designed by plastic pipes with the diameter ranging from 250 to 300 mm. We evaluate the proposed algorithm using 74 images in 3 different sewer pipes with 3 types of manholes, inlets and joints. The image has $704 \times 480$ pixels and is captured manually from video frames (Fig. 4.10).

Table 4.1 presents the percentage of correctly computed distance in comparing with the real distance. Here the distance error less than 5cm is assumed to be correct. On the average about 100% of input sewer image provides correct distance.

Table 4.1: Performance of self localization computing with error less than 5cm.

| Images type | The number of images | Rate(%) |
|:---:|:---:|:---:|
| Manhole | 28 | 100 |
| Joint | 28 | 100 |
| Inlet | 18 | 100 |
| Total | 74 | 100 |

## 4.5 Conclusions and discussions

We have presented a method for self localization and landmarks detection of an autonomous sewer robot in sewer pipes based on fusion of data from an IR sensors and a single camera. It is capable of self localization, which cannot
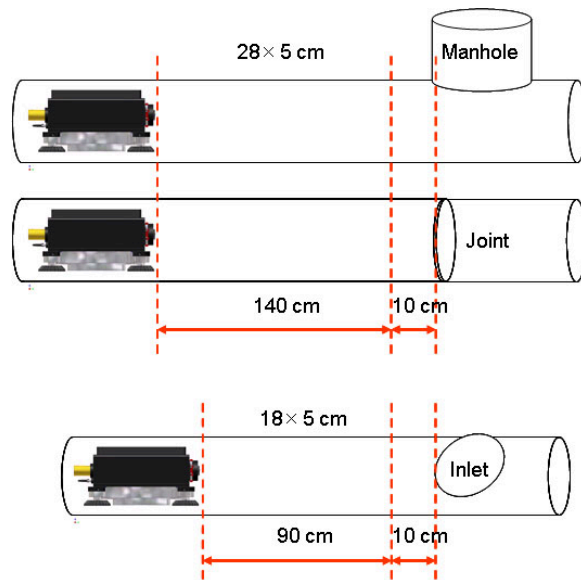
Figure 4.10: Location of captured images using in our experiments.

be done by conventional methods. We also conducted experiments for sewer robot navigation in a dry sewer test field at FAIS-RDSO, Kitakyushu. They succeed in detecting local features by using sensory information.

Based on these experimental results, we can say single camera as a vision sensor is suitable for fault detection and navigation purposes. In additional, we also test the stereo camera to observe the performance of navigating, which is described in next chapter.

# Chapter 5

# Navigation based on stereo camera and laser scanner

## 5.1 Introduction

Robot localization and navigation is one of the fundamental issues involved in robotics. Using different type of sensors such as ultrasonic sensor, camera and laser scanner, by mean of sensor fusion, to compile information about robots location is applied to a wide range of the robot task. With the restriction of the environment, the task of detemining the robot position can be pose a wide range of problems and difficulties. Dynamic, fast changing environmets, moving obstacles as well as potential noisy sensor information make the position estimation task very difficult.

The present environment of a sewer system facilitates this task to some degree, since boundary restrictions in the environment eliminate a number of problems. Due to the closed geometry, drifting of the robot does not occur to such a highlight degree, moving obstacles do not occur. Further the limited number of distinct local features such as manholes, junctions, pipe joints and inlets make their identification easier.

In this chapter, firstly, we propose two stereo matching method, which is suitable for sewer images. Then, we propose a navigation method using a parts of first proposed method and laser scanner data for detecting landmarks and estimating the location of a mobile robot.

## 5.2 Design of a new mobile laser scanner

It is difficult to use the conventional laser scanner on mobile robots such as KANTARO because of its size and weight. Therefore, we design the new laser

Figure 5.1: The newly developed laser scanner.
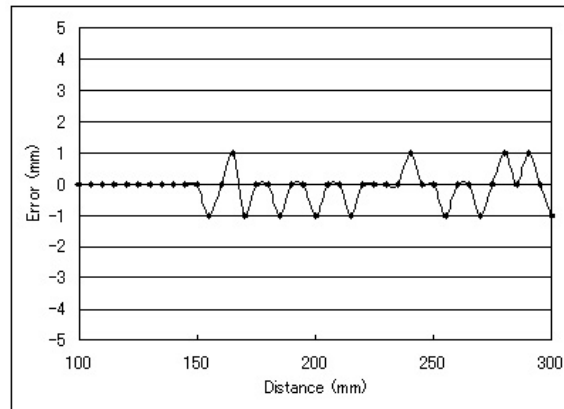


Figure 5.2: Errors in distance measurement.

scanner in Fig. 5.1 for Kantaro. The sensor is mounted on the rear-center of KANTARO and IR beam is emitted from the top of a rotary segment. The microcontroller calculates the distance, the laser scanner angle and so on. Data are transmitted to a computer at the sampling speed of 10KHz via the network with the maximum transmission rate of 1Mbps. Fig. 5.2 illustrates the errors in distance measurement. Table 5.1 describes the specification of the 2D laser scanner.

The diameter of the typical manhole is larger than that of the connected pipe by 50cm, and inlet size is between 10 and 15cm. Sewer landmarks are not uniformly distributed along the pipe perimeter. Rather, they appear in the upper part, left side and right side of pipes. This allows to restrict the search to the angle width of 15 degrees for each candidate as shown in Fig. 5.3, and to design the size and position of each scanning window. By full rotation of the laser scanner, the mirror rotates 360 degrees and the distance is measured at the right, top and left scanning windows.

47
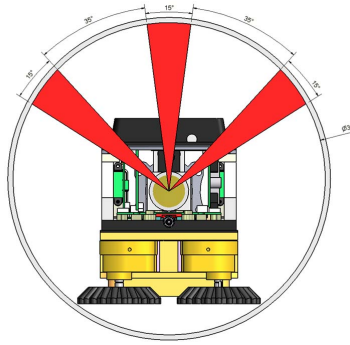
Figure 5.3: Scanning directions.

Table 5.1: Specification of the laser scanner.

| Scanning directions | 360 degree |
|---|---|
| Scanning speed | 0-1800 (rpm) |
| Distance range | 70-190 (mm) |
| Accuracy | $\pm 1$ (mm) |
| Beam radius | 0.5 (mm) |
| Transmission method | Full duplex serial transmission (2Mbps) |
| Sampling speed | More than 10 KHZ |
| Measured signals output | Distance, Scanning angle |
| Weight | 200 g |
| Size | $37 \times 48 \times 166$ (mm) |
| Power | $\pm 12V(0.5A) +5V(1A)$ |

## 5.3   A cooperative stereo matching algorithm

As is well known, stereo matching is an essential issue in computer vision. An excellent survey by Scharstein et al. [39] grouped existing approaches into orders, introduced an evaluation metric, and provided data for comparative studies. They also presented the rankings for most stereo matching algorithms at Middlebury website [45]. Most of them are based on segmentation, graph cuts [46]-[50] and other computational techniques [51]-[53]. Some of these methods have attracted much attention due to their excellent experimental results.

Segmentation is made based on the assumption that disparities are almost the same in one segment. The graph cuts method is also based on the same assumption. However, because the disparities change gradually in the sewer image, it is hard to segment the sewer image based on this assumption.

(a)Image of sewer inside        (b)Segmentation of (a)
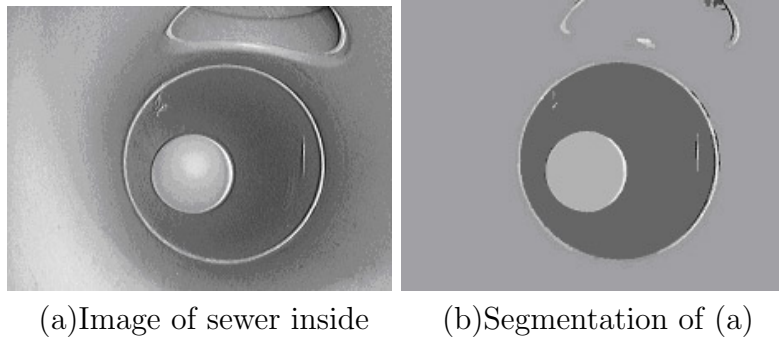
Figure 5.4: Sewer image and its segmentation.

We used a powerful segmentation algorithm named a shift mean algorithm [40] for the sewer image. It overcomes the difficulty of the gradual change of disparities. Fig. 5.4 show the images of sewer inside and the resulting segments, respectively. Due to the lack of illumination in the distant area, a large dark area always exists in the central part of the sewer image. This dark area in the sewer image tend to cause wrong segmentation. Furthermore, methods based on segmentation and graph cuts cost much computational time, hence do not have real-time characteristics. Although realtime stereo matching algorithms based on correlation, dynamic programming and other methods [54]-[56] have been proposed, they also suffer the above mentioned difficulties. Accordingly, they are not effective for the sewer image, either.

The above characteristics necessitate a suitable method which is fast and effective in our sewer environment. Scharstein describes a simple yet powerful method [41] to perform stereo matching for a feature group using the gradient of the images. This method provides a strong response in the edge part. He also claims that the ramp image can only be matched by comparing absolute brightness [42].

## 5.3.1   Proposed algorithm

It is desired that a stereo matching process in a sewer system be robust in both the feature group and the non-feature group. In other words, the feature group such as edges and cracks be clearly visible, and the matching measures in both groups be accurate. The computational time should also be small, i.e., in seconds. The proposed algorithm, which satisfies these requirements, is described below. We proposes a new cooperative algorithm using a new matching measure of linear computation (hereafter referred to as LC) for a feature group and the conventional Sum of Squared Differences (SSD) with constraints for a non-feature group [76]. In this algorithm, the reference

49
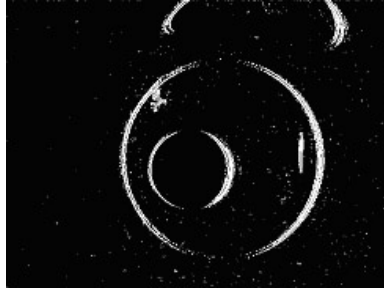
Figure 5.5: Classification of groups.

image is divided into the feature pixel group and the non-feature pixel group. The LC measure, which has similarity with the gradient but requires less computational cost, is used in the feature group, and the conventional SSD with neighboring similarity and other constraints is applied to the non-feature group.

**Group classification**

At this stage, pixels are divided into two groups by setting a threshold for group classification, $T_0$. We can also regard this stage as a simple but special segmentation that classifies the image into a feature "region" and a non-feature "region." In Fig.5.5, the light pixels constitute the feature region and the dark pixels constitute the non-feature region. The difference between two neighboring pixels, $D(x, y)$, is given by:

$$D(x, y) = \mid I(x, y) - I(x - 1, y) \mid \tag{5.1}$$

where $I(x, y)$ is the brightness of the pixel at $(x, y)$. If $D(x, y) \geq T_0$, the pixel, $(x, y)$, is treated as a feature pixel, else it is treated as a non-feature one.

**Matching of feature pixels**

We first applied the conventional gradient measure for stereo matching [41] to our sewer image. The resulting disparities provide the distance map using the geometry of a stereo camera [57]. This distance map is represented by the brightness of pixels; the larger the distance is, the darker the pixel is. However, because of the shadow, we found that the conventional gradient measure produced some fringes of the edges and cracks in the distance map as in Fig. 5.6(a).

To overcome this difficulty, we propose a new measure which is partly similar to the conventional gradient measure. To compare locations in two images, most existing methods depend on *similarity* reflecting the resemblance of the corresponding locations of two images, and sometimes on *distinctiveness* reflecting the likelihood of the correctness of the match. Our measure combines the similarity and the distinctiveness into a single measure of matching. Since only the horizontal shifts need to be considered in the stereo matching, the differences of the brightness between horizontally neighboring pixels are calculated. The differences between two neighboring pixels in left-eye and right-eye images are $D_L(x,y) = I_L(x,y) - I_L(x-1,y)$ and $D_R(x,y) = I_R(x,y) - I_R(x-1,y)$, respectively.

We calculate the sum of their absolute values, $C_d(x,y) = |D_L(x,y)| + |D_R(x+d,y)|$, to represent the distinctiveness, and the minus of the absolute value of their difference, $-G_d(x,y) = -|D_L(x,y) - D_R(x+d,y)|$, to represent the similarity at the displacement, $d$. We define the matching measure as the sum of these two terms: $E_d(x,y) = C_d(x,y) - G_d(x,y)$. In summary, for a given displacement, $d$, the matching measure, $E_d$, is:

$$E_d(x,y) = |D_L(x,y)| + |D_R(x+d,y)| - |D_L(x,y) - D_R(x+d,y)| \quad (5.2)$$

To find the best match for an isolated pixel, we maximize $E_d$ with respect to $d$ under consideration. It is not hard to understand why our method generates strong responses at the feature pixels. If the matching pixel is a non-feature one, the difference of brightness between horizontally neighboring pixels is small. As a result, both $D_L(x,y)$ and $D_R(x+d,y)$ have small values. Hence, $E_d$ also has a small value. On the contrary, if the matching pixel is a feature one, it has a large difference of brightness horizontally. This will result in a large value of $E_d$. Therefore, this method is expected to work well in the matching of feature pixels.

Fig.5.6 demonstrates that the resulting distance map by the proposed measure provides better view of the feature pixels than that by the conventional gradient refined measure.

## Matching of non-feature pixels

At this stage we use the conventional SSD with constraints for the matching of non-feature pixels for the following two reasons. Firstly, Scharstein [42] presented that a pair of ramp images have no local texture variation, hence have constant gradient almost everywhere except for the boundaries. A pair of two images can only be matched by comparing the absolute brightness, hence any algorithm based on band-pass filters or gradient will fail (as is the
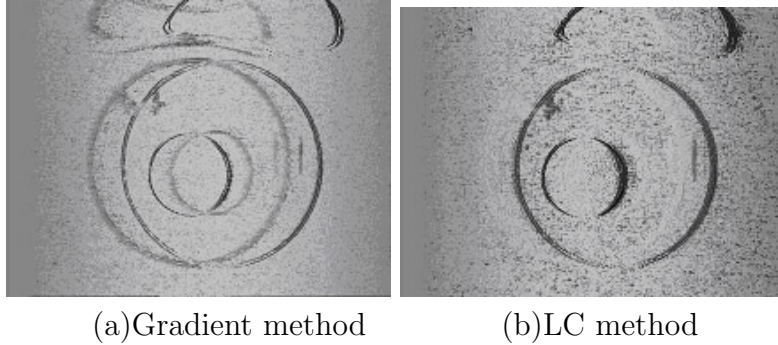
(a)Gradient method          (b)LC method

Figure 5.6: Distance maps.

human visual system). The other reason for the choice of the SSD is its small computational cost, because SSD is a simple area-based algorithm.

The best match with a given pixel in the image is found by comparing a square window centered at this pixel against the windows of the same size centered at the corresponding candidate pixels in the other image. The sum of the squared differences of brightness between the windows is used as a measure of dissimilarity. The pixel with the minimum dissimilarity is considered to be the best matching pixel.

In the proposed algorithm, we introduce constraints to reduce matching error based on the following assumptions. Marr and Poggio [43] [44] first introduced assumptions in stereo matching to the effect that the disparity has a unique value and is continuous almost everywhere. These assumptions are also applicable to our case.

For the resulting disparity, $d$, we modify it by imposing a neighboring constraint based on the position of pixels. It is assumed that if two pixels are adjacent neighbors, they have similar disparities.

If the difference between disparities of two neighboring pixels is larger than an empirically set threshold, $T$, we modify the disparity of the current pixel as:

$$d_m = d_{pre} + sgn(d_{cur} - d_{pre}) \times T/2 \qquad (5.3)$$

where $d_m$ is the modified disparity, $d_{cur}$ and $d_{pre}$ are the disparity at the current pixel and that at the immediate left pixel, respectively. The sign function, $sgn(x)$, is defined as:

$$sgn(x) = \begin{cases} +1 & if x \geq 0 \\ -1 & else \end{cases} \qquad (5.4)$$

The calculation of the disparity involves correlating the window for the left-eye image with those for the right-eye images with various disparities,

52

*d.* Fig.5.7 illustrates the relation between the value of the matching measure and the disparity. Let the curve over disparity axis be called a matching measure curve here. The disparity at which the matching measure is the smallest corresponds to the pixel with the largest matching. In areas with non-salient texture, a matching measure curve becomes nearly flat over the disparity axis. A matching measure curve with multiple minima suggests a repetitive texture.
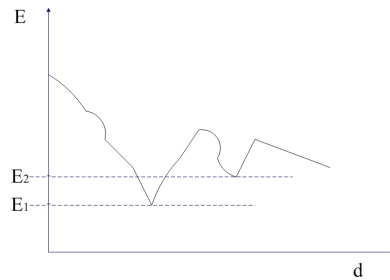


Figure 5.7: Values of the matching measure, $E_d(x, y)$.

Noises in the image tend to cause wrong decisions. Let $E_1$ at $(x_1, y_1)$ be the smallest measure value, and $E_2$ at $(x_2, y_2)$ be the second smallest measure value, and $(x_1, y_1)$ is not adjacent to $(x_2, y_2)$. The relative difference of the measure can be defined as:

$$E_d = (E_2 - E_1)/E_1 \tag{5.5}$$

Almost the matching measure values represent a curve with a few changes, because the disparities change gradually in the sewer image. A large $E_d$ means that the smallest measure value is far from the second smallest measure value, which can be caused by a noises in the image. In order to overcome this difficulty, if $E_d$ is bigger than a threshold for function value constraint $T_e$, we choose $E_2$ instead of $E_1$ as the best matching measure. The threshold $T_e$, is set empirically.

## 5.3.2 Experimental results

To evalute the effectiveness of the proposed algorithm, we capture the stereo images in Figs. 5.8 and 5.9 in the dry sewer test field (Fig. 4.9), which is made by plastic pipes with the diameter ranging from 250 to 300mm. The former pair in Fig. 5.8 are under bright illumination and the latter one in Fig. 5.9 are under dimmed illumination.
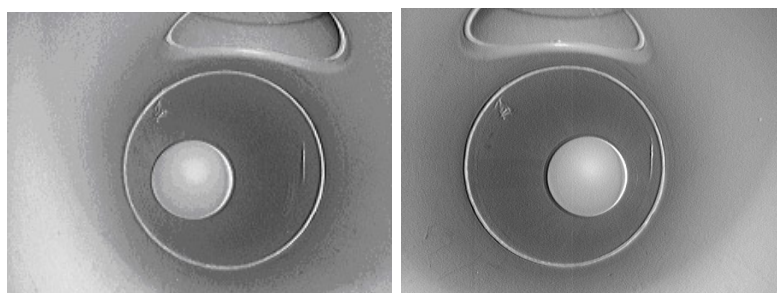
(a)Left image          (b)Right image

Figure 5.8: The first pair of stereo images under bright illumination in our experiment.
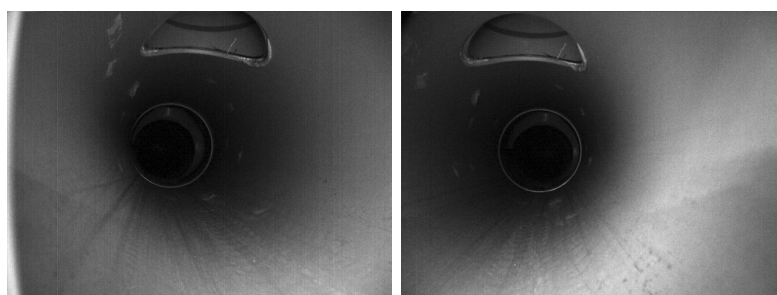


(a)Left image          (b)Right image

Figure 5.9: The second pair of stereo images under dimmed illumination in our experiment.

Firstly, we use a Gaussian filter for smoothing the images to reduce quantization errors and noises. The image is $640 \times 480$ pixels. Values of parameters used in the experiment are:

a) Threshold for classification of groups, $T_0$: 10;

b) Threshold for function value constraint, $T_e$: 0.2;

c) Threshold for neighboring constraint, $T$: 10;

d) The window size for SSD is $7 \times 7$ pixels.

We randomly choose a rectangle of $8 \times 8$ pixels comprising both the feature and the non-feature pixels near the manhole, and obtain the distance map from them. A PC of Pentium4 with 3.0GHz and 1.0GB memories is used here. The distance error in the experiment is given by:

$$error = |d - d_0| \tag{5.6}$$

where $d_0$ is the real distance from the camera to a point under consideration in the sewer. The distance error in Fig.5.10 is the average over two pairs

54
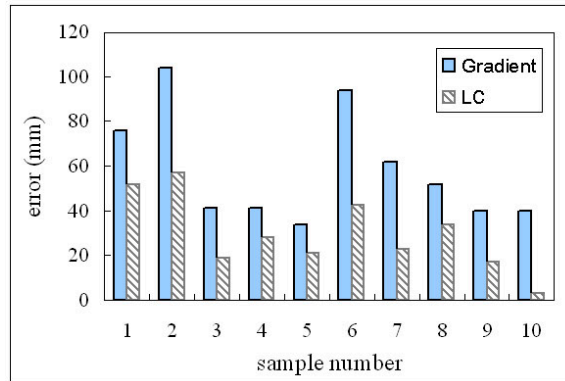
Figure 5.10: Distance errors in feature pixels.
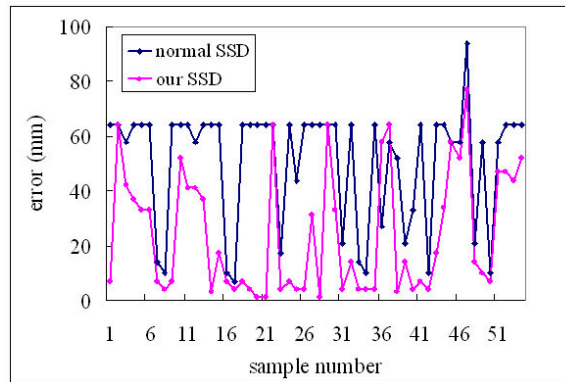


Figure 5.11: Distance errors in non-feature pixels.

of stereo images using the gradient and LC in the feature pixels. The distance error using our LC measure is significantly smaller than that by the conventional Gradient measure in the feature pixels.

Fig. 5.11 illustrates the distance error using the conventional SSD and the proposed SSD with constraints in the non-feature pixels. The proposed SSD with constraints also significantly decreases the distance error compared with the conventional SSD in the non-feature pixels. Fig. 5.12 presents the average computational time over 10 trials using the above four measures. The computational time by the LC measure is about 1/5 compared with that by other measures.

### 5.3.3  Conclusions

We have developed a cooperative stereo matching algorithm using SSD and LC measures and it can be implemented in a navigation system. It is a ro-
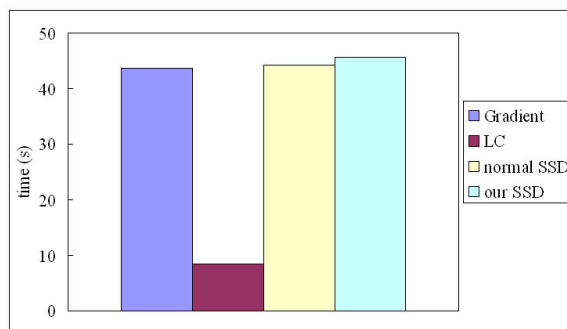
Figure 5.12: Computational times.

bust algorithm for sewer inspection in robot vision. The algorithm produces an easy-to-understand distance map of the sewer, emphasizing the feature region. The computational time by this algorithm is about 1/5 compared with that by other algorithms such as the conventional SSD.

## 5.4 A fast stereo matching algorithm using interpolation

In section 5.3, we proposed a suitable cooperative stereo matching algorithm for autonomous inspection robots. The proposed method is shown a good performance in computational time, but, for real-time execution of a task by inspection robots, a fast algorithm is desired.

Many conventional matching methods are exsist and some of them attracted much attention due to their excellent performance. However, we found that most of them are computationally expensive [50, 58, 59, 56, 42, 52, 53, 48]. Although several real-time stereo matching algorithms based on correlation, dynamic programming and other methods [47, 54, 60] have been proposed, they are not effective enough for sewer images. Mayer describes a simple yet powerful algorithm [61] to perform stereo matching by combining many methods. It attracted attention due to its simplicity and good performance in stereo matching. Although, it is applicable to our case, it does not work in real-time.

In this section, we propose a fast algorithm using cubic interpolation and providing superior performance for autonomous inspection robots [67]. The proposed algorithm is regarded as a combination of a revised Mayer's algorithm and interpolation. At the outset, an image is divided into many blocks. Then, a combined measure of the Sum of Squared Differences (SSD) and cross-correlation is calculated at only the four corner points of the blocks.

56

A downsampled sewer disparity image is composed of only the corner points. Finally, we extend the downsampled sewer disparity image into a regular-sized disparity image by the cubic interpolation [62], taking advantage of continuous change of disparities in the sewer environment.

## 5.4.1  Proposed algorithm

Stereo matching in sewer system is expected to be robust and efficient. The proposed algorithm provides high accuracy with small computational cost. The overview of the proposed algorithm is shown in Fig. 5.13. It is composed of two major parts: a combined measure using the SSD and the cross-correlation, and the cubic interpolation for extending a downsampled sewer disparity image into a regular-sized sewer disparity image. In the first part, we divide an image into $8\times 8$ blocks. Then, a combined measure of SSD and the cross-correlation is applied to the four corner points in each block. A downsampled sewer disparity image is composed of only the corner points. In the second part, we use the cubic interpolation [62] for extending the downsampled sewer disparity image into a regular-sized sewer disparity image.

### Combined measure

Scharstein claimed that a ramp image can only be matched with other images by comparing absolute intensities or correlation [39]. In our case, a sewer image can be treated as a ramp image. Mayer [61] found that the performance of SSD was in almost all cases worse than that of absolute differences. He used truncated differences in calculating absolute differences. Finally he found that failure characteristics based on normalized cross-correlation seem to be different from those based on absolute differences, and suggested that it might be useful to combine both.

We utilize this finding in our proposed method. We define the following SSD matching measure, $SSD_d(x,y)$, for a disparity, $d$.

$$SSD_d(x,y) = \sum_{i=0}^{M-1} \sum_{j=0}^{N-1} (I_L(x+i,y+j) - I_R(x+i+d,y+j))^2 \qquad (5.7)$$

where $I_L(x,y)$ and $I_R(x,y)$ are the brightness of the pixel at $(x,y)$ in the left image and right image, respectively. $M$ and $N$ are the number of vertical pixels and that of horizontal pixels of the window, respectively.

We, then, define the $SSD'_d(x,y)$ by $1 - SSD_d(x,y)/pa$, where $pa$ is a parameter for adjusting the influence of $SSD_d(x,y)$. To find the best match for
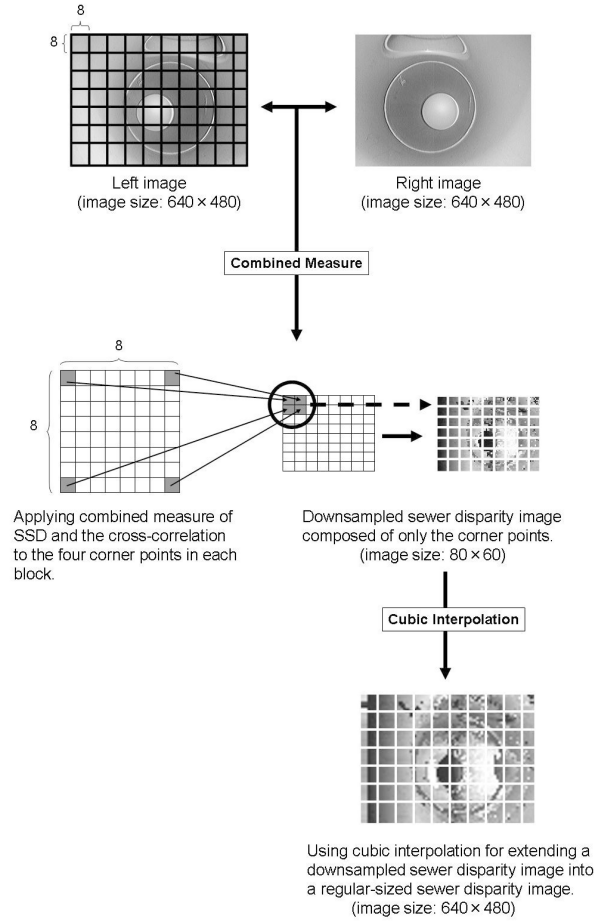
Figure 5.13: Overview of the proposed algorithm.

an isolated pixel, we maximize $SSD'_d(x, y)$ with respect to $d$ under consideration. Among all possible disparity for the pixel $(x, y)$, the one that gives the maximum $SSD'_d(x, y)$ is selected as the estimated disparity by $SSD$.

$$disparity_{SSD'}(x, y) = argmax_d \left\{ SSD'_d(x, y) \right\} \qquad (5.8)$$

We define the following cross-correlation, $Cor_d(x, y)$, between right and left images.

$$Cor_d(x,y) = \frac{\sum_{i=0}^{M-1}\sum_{j=0}^{N-1}(left-\bar{A_L})(right_d-\bar{A_{R_d}})}{\sqrt{\sum_{i=0}^{M-1}\sum_{j=0}^{N-1}(left-\bar{A_L})^2 \times \sum_{i=0}^{M-1}\sum_{j=0}^{N-1}(right_d-\bar{A_{R_d}})^2}}$$

$$left = I_L(x+i,y+j), \quad right_d = I_R(x+i+d,y+j)$$

$$\bar{A_L} = \frac{1}{M \times N}\sum_{i=0}^{M-1}\sum_{j=0}^{N-1}I_L(x+i,y+j)$$

$$\bar{A_{R_d}} = \frac{1}{M \times N}\sum_{i=0}^{M-1}\sum_{j=0}^{N-1}I_R(x+i+d,y+j)$$

(5.9)

We maximize $Cor_d(x,y)$ with respect to $d$ to find the best match and define the following estimated disparity by cross-correlation.

$$disparity_{Cor}(x,y) = argmax_d\{Cor_d(x,y)\} \tag{5.10}$$

Because cross-correlation works better for strong texture regions with large horizontal gradient, we give a weight $\omega$ to $disparity_{Cor}(x,y)$ by;

$$\omega = \frac{G_h}{G_0} \tag{5.11}$$

where $G_h$ is horizontal gradient and $G_0$ is that for the standard case. The combined measure $Com_d(x,y)$ and the corresponding estimated disparity are computed at the four corner points in each block by the following equation.

$$Com_d(x,y) = \frac{SSD'_d(x,y) + \omega Cor_d(x,y)}{1+\omega}$$

$$d(x,y) = argmax_d Com_d(x,y) \tag{5.12}$$

$$d(x,y) = \frac{disparity_{SSD'}(x,y) + \omega disparity_{Cor}(x,y)}{1+\omega}$$

Finally, the downsampled sewer disparity image composed of only the corner points is represented by the following equation. Then, we use cubic interpolation to extend the downsampled sewer disparity image in the following subsection.

$$disparity(x,y) =$$

(a)Downsampled disparity image  (b)Nearest-neighbor interpolation

(c)Linear interpolation          (d)Cubic interpolation
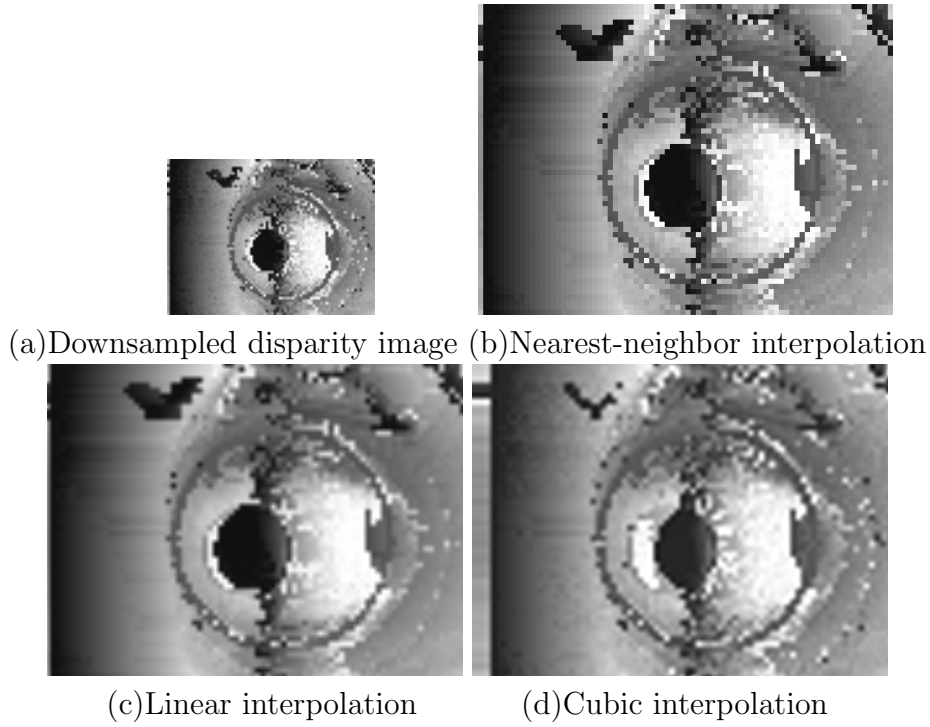
Figure 5.14: Different interpolation images of downsampled sewer disparity image.

$$
\begin{bmatrix}
d_s(0,0) & d_s(7,0) & \cdots & d_s(640,0) \\
d_s(0,7) & d_s(7,7) & \cdots & d_s(640,7) \\
\vdots & \vdots & \ddots & \vdots \\
d_s(0,480) & d_s(7,480) & \cdots & d_s(640,480)
\end{bmatrix}
$$

(5.13)

where $d_s(x,y)$ at the corner points are given by Eq. 5.12.

**Interpolation**

Interpolation techniques are used to estimate disparities at pixels other than the corner points by extending the downsampled sewer disparity image. There are various interpolation methods such as linear interpolation, nearest-neighbor interpolation and cubic interpolation. The simplest method among them is linear interpolation, but it is not very precise. The nearest-neighbor interpolation method assumes that the value of a point equals that of its nearest neighbor point. The cubic interpolation is the simplest method that provides smooth change in disparities using a polynomial of the third order.
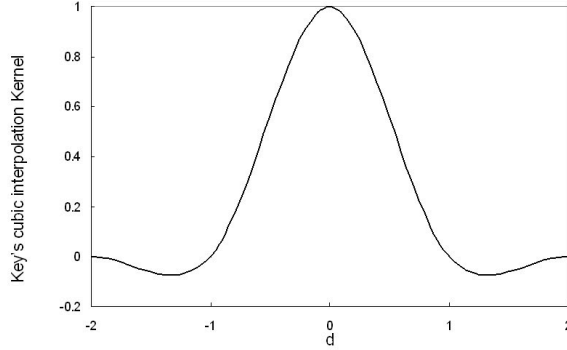
Figure 5.15: Key's cubic interpolation kernel.

We evaluate these interpolation methods in interpolating the downsampled sewer disparity image shown in Fig. 5.14. The cubic interpolation provides smooth change in disparities in sewer environment. In order to obtain smoother interpolation, several alternative interpolants have been proposed. The cubic interpolation kernel proposed by Keys [62] is given by the following equation and is shown in Fig. 5.15.

$$
\begin{cases}
f_0(d) = \frac{3}{2}|d|^3 - \frac{5}{2}|d|^2 + 1, & if\, 0 \leq |d| \leq 1 \\
f_1(d) = -\frac{1}{2}|d|^3 + \frac{5}{2}|d|^2 - 4|d| + 2, & if\, 1 \leq |d| \leq 2 \\
0, & else
\end{cases}
\tag{5.14}
$$

where $d$ is the distance between a pixel to be estimated and one of the surrounding 16 pixels. An example of the calculation of the new pixel value is shown in Fig. 5.16. To compute diparity value at $(x, y)$, we use the surrounding 16 pixels with known disparity values in the downsampled sewer disparity image. Note that fig.5.16 uses local coordinate system in contrast to global coordinate system in Eq.(5.13). As shown in Fig. 5.16, firstly, the average disparity value for each horizontal line is calculated by Eq.(5.15), where $f_1(d)$ and $f_0(d)$ are given by Eq.(5.14).

$$
\begin{aligned}
d_{ave}(1, y) &= d_s(1, 1) \times f_1(1.7) + d_s(1, 2) \times f_0(0.7) \\
&\quad + d_s(1, 3) \times f_0(-0.3) + d_s(1, 4) \times f_1(-1.3) \\
d_{ave}(2, y) &= d_s(2, 1) \times f_1(1.7) + d_s(2, 2) \times f_0(0.7) \\
&\quad + d_s(2, 3) \times f_0(-0.3) + d_s(2, 4) \times f_1(-1.3) \\
d_{ave}(3, y) &= d_s(3, 1) \times f_1(1.7) + d_s(3, 2) \times f_0(0.7) \\
&\quad + d_s(3, 3) \times f_0(-0.3) + d_s(3, 4) \times f_1(-1.3)
\end{aligned}
$$

61
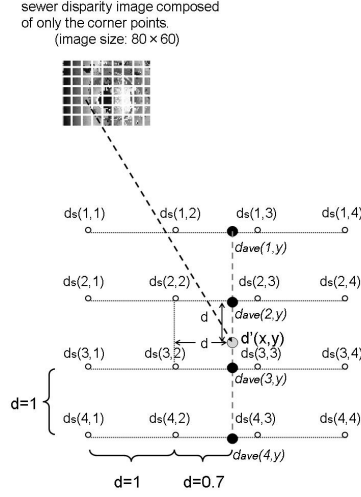
Figure 5.16: An example of the calculation of the new pixel value.

$$
\begin{aligned}
d_{ave}(4, y) &= d_s(4,1) \times f_1(1.7) + d_s(4,2) \times f_0(0.7) \\
&\quad + d_s(4,3) \times f_0(-0.3) + d_s(4,4) \times f_1(-1.3)
\end{aligned}
$$
(5.15)

Secondly, we use the average disparity value of the four new value, $d_{ave}(1, y)$, $d_{ave}(2, y)$, $d_{ave}(3, y)$ and $d_{ave}(4, y)$, to compute the disparity value at new pixel $d'(x, y)$, as follow.

$$
\begin{aligned}
d'(x, y) &= d_{ave}(1, y) \times f_1(1.7) + d_{ave}(2, y) \times f_0(0.7) \\
&\quad + d_{ave}(3, y) \times f_0(-0.3) + d_{ave}(4, y) \times f_1(-1.3)
\end{aligned}
$$
(5.16)

## 5.4.2   Experimental results

To evaluate the performance of the proposed algorithm, we use two stereo images shown in Figs.5.17 and 5.18. The images in Fig. 5.17 are under bright illumunation and the images in Fig. 5.18 are under dimmed illumination.

Before matching, we first use a gaussian filter (windows size $7 \times 7$, $\sigma = 3$) for smoothing the images to reduce quantization errors and noises. The image is $640 \times 480$ pixels. Values of parameters used in the experiment are as follows:
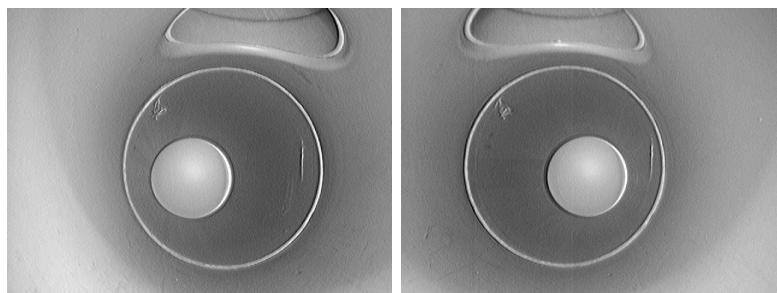
(a)Left image         (b)Right image

Figure 5.17: The first pair of stereo images of sewer pipe under bright illumination.
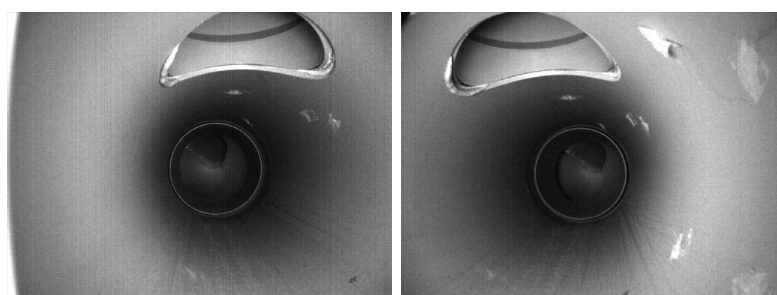


(a)Left image         (b)Right image

Figure 5.18: The second pair of stereo images of sewer pipe under dimmed illumination.

1. We divide image into several 8×8 blocks;

2. The window size for calculating both the SSD and the cross-correlation is 7×7 pixels.

3. Weighting parameter $G_0$ is 32.

Fig. 5.19 illustrates the disparity images obtained by the conventional SSD, the cross-correlation and the proposed method under bright and dimmed illumination . To evaluate the error of the distance, we randomly choose a set of pixels near the feature area such as the manhole in the images. Then distance error in the experiment is given by;

$$error = |d - d_0| \qquad (5.17)$$

where $d_0$ is the real distance between the camera and a point under consideration in the sewer and $d$ is the corresponding estimated distance. The

distance errors of various methods are shown in Fig. 5.20. The distance errors by our method is significantly smaller than those by other conventional methods.



(a)The conventional SSD
(under bright illumination)

(b)The conventional SSD
(under dimmed illumination)

(c)The cross-correlation
(under bright illumination)

(d)The cross-correlation
(under dimmed illumination)

(e)The proposed method
(under bright illumination)

(f)The proposed method
(under dimmed illumination)
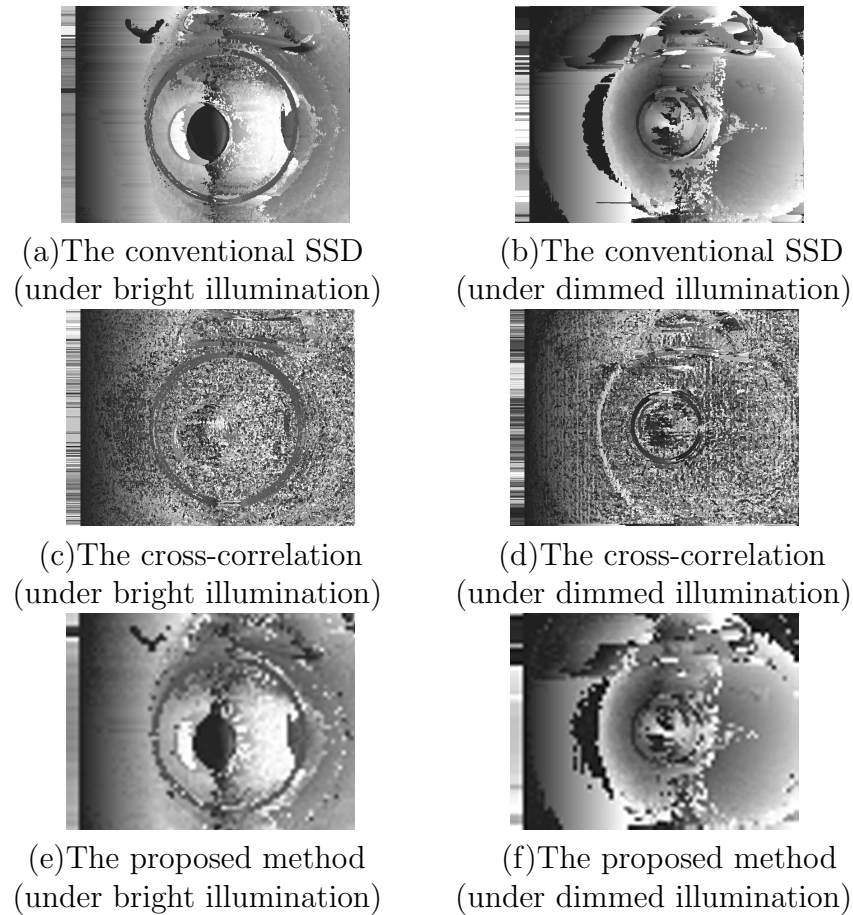
Figure 5.19: Disparity images.

We also evaluate the distance errors for different interpolation methods in our proposed method in Fig.5.21. NN (nearest-neighbor) has much larger error than those by linear and cubic interpolation. Also the error of cubic interpolation is smaller than that of linear, but not much difference in computational time as shown in Table 5.2. Here, we focus on the distance error, hence choose the cubic interpolation in our method due to the smallness of distance errors.

Fig. 5.22 presents the average computational time using the above methods. The computational time by the our method is much smaller; only about 1/20 compared with those by other measures.
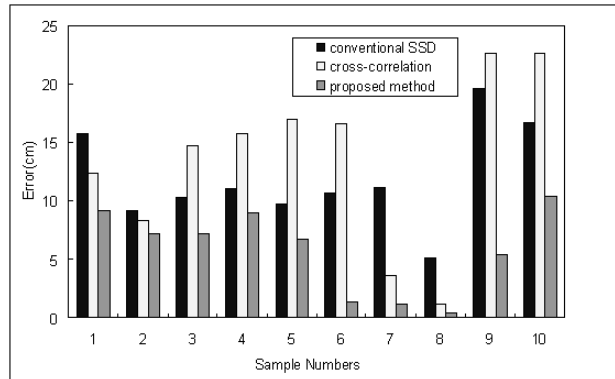
Figure 5.20: Distance errors of various methods.
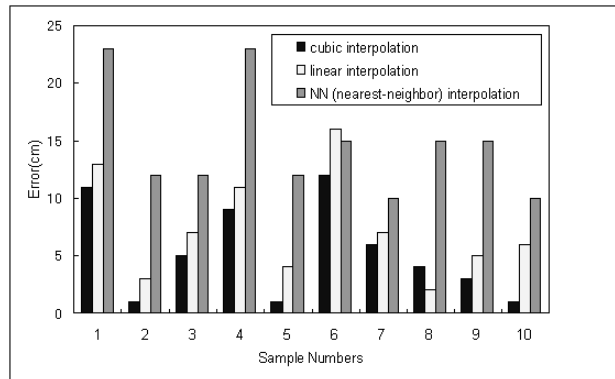


Figure 5.21: Distance errors for different interpolation methods in our proposed method.

### 5.4.3 Conclusions

We have developed a fast stereo matching algorithm using cubic interpolation in this paper. The algorithm successfully produces a good visible distance image of the sewer. Cubic interpolation drastically reduces the computational cost. The computational time by our algorithm is only 1/20 of those by the conventional algorithms such as the SSD. Hence it is suitable for our real-time sewer vision system. The average error of the sewer evidently decreased down to 5.3cm.

## 5.5 Fusion of camera and laser scanner

Sewer environment is composed of cylindrical pipes, in which only a few landmarks such as manholes, inlets and pipe joints are available for localization.

65

Table 5.2: Mean error and computation time.

| Measure | Mean error (cm) | Computation time (s) |
|---------|-----------------|----------------------|
| NN      | 14.7            | 6.1                  |
| Linear  | 7.4             | 6.4                  |
| Cubic   | 5.3             | 8.9                  |
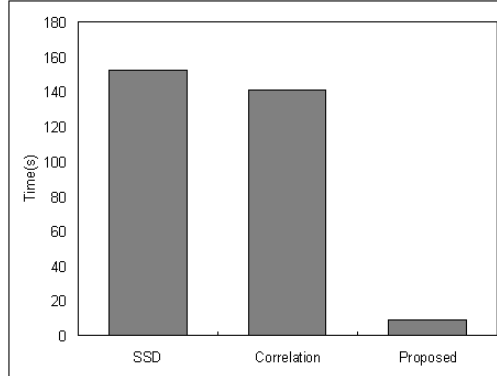


Figure 5.22: Comparison of computational time.

In this section, we present a method for navigation of an autonomous inspection robot in a sewer pipe system based on detection of landmarks [65, 71]. In this method, location of an autonomous sewer inspection robot in the sewer pipe system is estimated from stereo camera images. The laser scanner data are also used to ensure accurate localization of the landmarks and reduce the error in distance estimation by image processing. The method is implemented and evaluated in a sewer pipe test field using a prototype robot, demonstrating its effectiveness.

The proposed method in Fig. 5.23 is composed of two stages: estimation of the location of a mobile robot and detection of landmarks. Firstly, a stereo sewer image is captured by the stereo camera on KANTARO. Secondly, we extract two rectangular Region of Interest(ROI) images for the manholes, inlets and joints, and detect edges in each ROI image. Thirdly, a fast and accurate stereo matching measure (LC) is applied to these ROI images to estimate the distances between the robot and landmarks. Fourthly, we refine the estimated distances using a threshold elimination function. If the refined distance is less than 10cm, we check the laser scanner data to detect the landmark. Finally, the refined estimates of location of the robot and the landmarks are used for navigation.
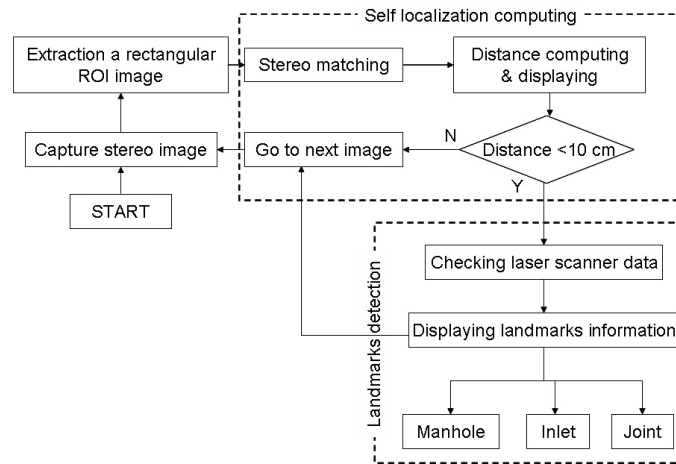
Figure 5.23: Overview of the proposed method.



(a)The rectangular ROI image
for the manhole and inlet

(b)The rectanglular ROI
image for the joint
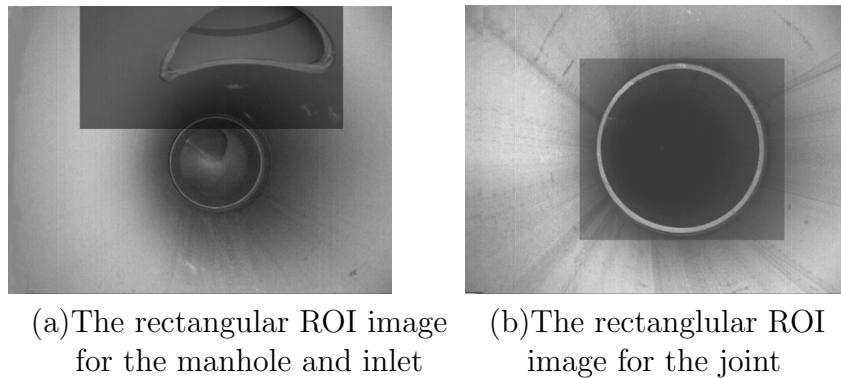
Figure 5.24: Original image and the extracted rectangular ROI images.

**Edge detction in extracted rectangular ROI image**

In sewer pipe systems, manholes, inlets or joints are always located in particular parts of the sewer image; the manholes and inlets are always in the upper part of the sewer image, and the joints are always in the central part of the image. Fig. 5.24 illustrates the original image and the extracted rectangular ROIs of manholes, inlets and joints.

After the extraction of ROI, we use the canny edge detector to get the edges in ROI. The Canny edge detection algorithm [63] is known to be the optimal edge detector in terms of error rate. It introduced two kinds of threshold for the gradient with hysteresis, i.e., the lower threshold $T_1$ and the higher threshold $T_2$. The values of the threshold are determined based on the following requirements. The first requirement is that edges in im-

ages should not be overlooked and that non-edges should not be detected as edges. The former corresponds to the error of the second kind, and the latter corresponds to the error of the first kind in mathematical statistics. The second requirement is that the edges be well localized. In other words, the distance between the detected edge and the actual edge be minimum. The third requirement is to produce only one response to each edge. This is included because the first two are not enough to eliminate multiple responses to an edge.

Based on these requirements, the canny edge detector firstly filters the image to eliminate noise. It then finds the image area with large spatial derivatives. The algorithm then tracks along these regions and any pixel in an edge list with the gradient larger than the higher threshold is classified as a valid edge. Pixels connected to a valid edge and with the gradient larger than the lower threshold are also classified as an edge. The small value of the higher threshold tends to increase the number of spurious and undesirable edge fragments, hence should be avoided.

## Distance measurement by stereo matching

An application of the conventional gradient measure for stereo matching [41] to our sewer image generates disparities, which provide the distance map based on the geometry of stereopsis [57]. The resulting distance map is represented by the brightness of pixels; the larger the distance is, the darker the pixel is. Due to the shadow, however, the conventional gradient measure tends to produce fringes of the feature pixels in the distance map as in Fig. 5.6.

To overcome this difficulty, we propose a new measure (See 5.3.1) which is suitable for matching of feature pixels.

## Refinement of the measured distance

Fig. 5.25 illustrates two linear fits of the number of edge points by our method. For computing the linear fits, we use a plenty of training images. Firstly, the edges of training images are extracted by the Canny edge detector using two sets of thresholds for the gradient, $(T_{1_1}, T_{2_1})$ and $(T_{1_2}, T_{2_2})$. True distances between the camera and landmarks are measured manually, and are used for ground truth. Then, we make two linear fits between the number of edge points extracted by two sets of thresholds for the gradient and the corresponding true distance. Finally, a shorter distance $\tau_1$ is estimated by the linear fit in Fig. 5.25(a), given the number of edge points. Similarly, a longer distance $\tau_2$ is estimated by the linear fit in Fig. 5.25(b), given the

(a) $T_{1_1} = 50$ and $T_{2_1} = 150$    (b) $T_{1_2} = 50$ and $T_{2_2} = 250$
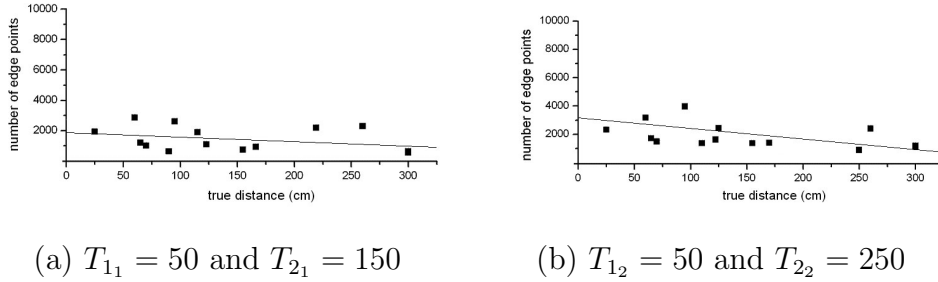
Figure 5.25: Two linear fits of the number of edge points for two sets of thresholds for the gradient.

number of edge points. These shorter and longer distances play a major role in the subsequent computation.

We can estimate the distance between the robot and each landmark by the stereo matching. We use the following threshold elimination function to obtain refined distance by averaging estimated distances.

$$\rho(x) = \begin{cases} x & (if \quad \tau_1 \leq x \leq \tau_2) \\ \tau_2 & (if \quad x > \tau_2) \\ \tau_1 & (if \quad x < \tau_1) \end{cases} \tag{5.18}$$

Suppose the estimated distances between the robot and features of a landmark are $D = \{d_1, \ldots, d_{N_f}\}$, where $N_f$ is the number of feature pixels in ROI image. The refined distance, $d_r$, is given by:

$$d_r = \frac{1}{N_f} \sum_{i=1}^{N_f} \rho(d_i) \tag{5.19}$$

**Detection of landmarks by a laser scanner**

At the last stage, we compute the distance between the robot and each landmark. In other words, when the robot reaches one of the landmarks, the distance becomes zero and the system can detect it. However, the computed distance based on stereo image still has some error, hence the laser scanner data are applied to improve its estimation. If the refined distance is less than 10cm, we regard that the robot is close enough to the corresponding landmark. Then, the system checks the laser scanner data for still better estimation.

As shown in Fig. 5.3, the laser scanner has three scanning windows at the right, top and left. During one rotation of the laser scanner, the IR beam passes three windows and provides three distance values. Table 5.3 gives

69

(a)The manhole          (b)Inlet at the right
side range of scanning
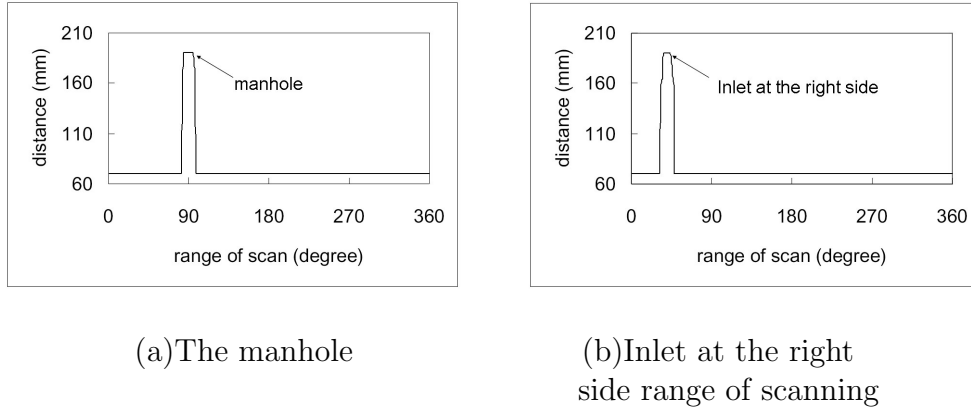
Figure 5.26: Typical landmarks detected.

estimation of landmarks based on the status of the distance measurements.
Our robot is designed for the pipes with the diameter ranging from 250
to 350mm. When the robot is moving inside the sewer pipe, the distance
measurement is between 125mm and 175mm. The distance value larger than
175mm is regarded as a distance measure at the landmarks.

Table 5.3: Estimation of the type of landmarks based on measurements.

| Status No. | Distance value larger than 175mm | Estimated landmark type |
|:---:|:---:|:---:|
| 0 | none | no landmark |
| 1 | at the top window | manhole |
| 2 | at the left window | inlet at the left |
| 3 | at the right window | inlet at the right |
| 4 | at the top and at the right or left window | manhole with junction |
| 5 | at the top, at the right window, and at the left window | robot is outside of the pipe |

Fig. 5.26 illustrates typical places where the KANTARO detects the
manhole and inlet in moving through the pipe with diameter 300mm. The
rotation starts from the horizontal line (counterclockwisely).

## 5.6 Experimental results

To evaluate the effectiveness of the proposed method, we did a series of
experiments by running the KANTARO in the sewer test field.

70
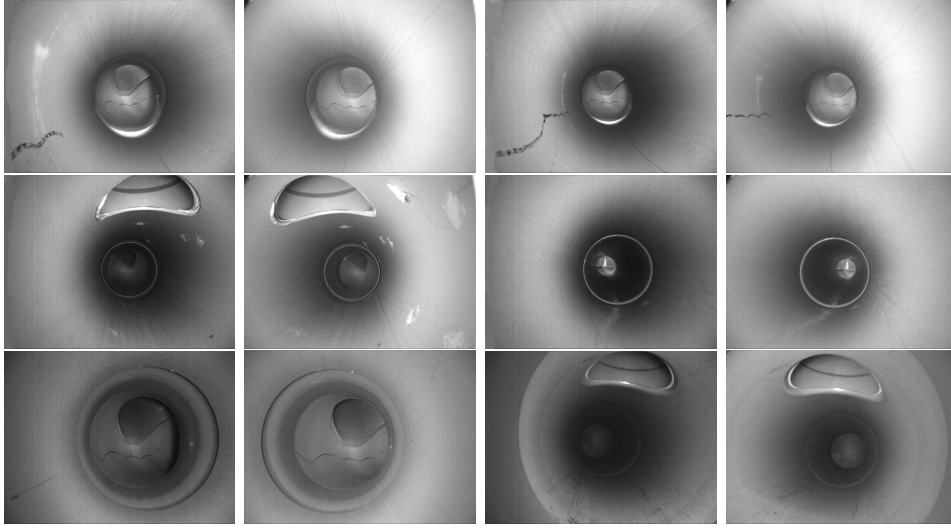
Figure 5.27: Samples of stereo images captured by KANTARO during its movement in the sewer test field.

**Self localization**

This test demonstrates the accuracy of self localization by capturing stereo images with size of $640 \times 480$ pixels such as shown in Fig.5.27. We used the lower threshold $T_1 = 50$ and the higher threshold $T_2 = 200$ for edge detection in each ROI images. Then the distance of feature pixels computed by LC measure. Next, we used two differents sets of thresholds value for the gradient, $(T_{1_1} = 50, T_{2_1} = 150)$ and $(T_{1_2} = 50, T_{2_2} = 250)$ for computing the linear fit, as shown in Fig. 5.25. Finally, the distance error between refind distance, $d_r$, and the true distance between the camera and a point under consideration in the sewer defined as the following;

$$error = |d_r - d'| \tag{5.20}$$

Table 5.4: The percentage of estimation of the distance with error less than 5cm.

| Images type | The number of images | Rate(%) |
|:---:|:---:|:---:|
| Manhole | 32 | 96.87 |
| Joint | 26 | 88.46 |
| Inlet | 12 | 91.66 |
| Total | 70 | 92.33 |

Table 5.4 presents the percentage of estimated distances with error less

71

than 5cm. On the average, about 92% of input sewer images provide the distances with small errors. Although the unstable illumination condition in the real sewer pipe system may effect a large errors in the estimation of the distance. We still have to perform further experiments to fine tune the values of parameters used for edge detection to reduce the errors.

**Navigation through sewer test field**



(a)Route 1          (b)Route 2
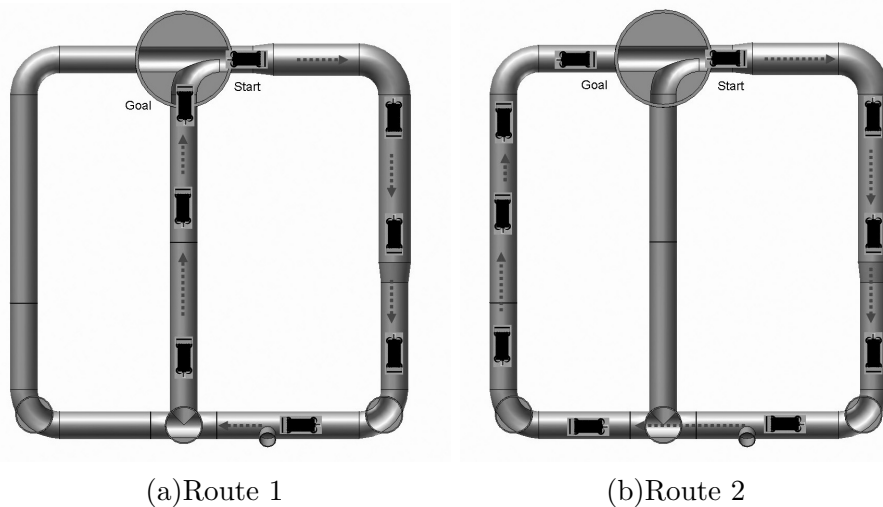
Figure 5.28: Examples of test navigation routes.

This test demonstrates KANTARO's ability in moving through a sewer pipe to the goal by using the proposed method. This experiment requires two basic perceptual abilities: detecting the landmarks and self localization. Both must be executed with high precision, because misperception such as turning action in straight pipe causes damage to KANTARO.

The mission of reaching the goal starting from the initial position is given by a human operator. Fig. 5.28 provides two different routes in navigation.

When the robot moves along the route 1, it makes a turning action at the first detected manhole with junction. Due to the position of the laser scanner on KANTARO, the manhole is detected when the robot fully entered into the manhole. At this moment, the robot can't turn, because the front wheel passed the junction entrance. To slove this problem, we modified the action as follows; if the robot enters into the manhole and is to turn it moves backward by 40cm and turns.

This mission is successfully achieved in our sewer test field with the maximum speed of 15cm/s.

## 5.7 Conclusions and discussions

We have proposed a method for navigation in sewer pipe systems using the robot platform, KANTARO. Our method uses stereo camera images and laser scanner data for detecting landmarks. It is capable of self localization of the sewer inspection robot, which cannot be done by the conventional methods. The results of self localization experiment shows high performance in providing the appropriate distance. We also design the new mobile laser scanner for KANTARO. The locations of landmarks in sewer pipe system are estimated successfully based on measurements. The laser scanner is fast enough to continuously scan relevant pipe sections in the presence of landmarks, while the KANTARO moves at ordinary inspection speed of up to 15cm/s. Also moving the KANTARO in our sewer test field by using the proposed method was done successfully.

# Chapter 6

# Conclusions

The purpose of this thesis is to elucidate the systems for detecting the faults automatically and navigating system for autonomous sewer inspection robot. The proposed systems can solve the "real-world" problems in civil robots, such as, support the operator and reduce the human error, tends to time and cost reduction. Below, I will summarize the contributions of the results from each chapter.

In section 3.3 of chapter 3, I proposed an intelligent system for detecting faulty areas automatically and implemented it in a real time system to solve the "real-world" problems in civil robots. In contrast to the conventional manual system, the proposed system can automatically detect faults and run in real time. The experimental results of proposed method in section 3.4 showed high detection performance, 100%, when the false positive rate is 34%. This ratio is acceptable for sewer inspection, and the reduction of time and cost are also realized.

The proposed method for navigation of an autonomous sewer inspection robot is described in section 4.3 of chapter 4. It is capable of self localization and landmark detection by using an IR and single camera sensors. In our method, the images are captured by a CCD camera at the front of a robot. The distance between robot and landmarks are estimated based on image data. The exact locations of the landmarks are compute by IR sensor data. Finally, information on the locations of a robot and landmarks are used for fault localization and robot navigation. We also conducted experiments for sewer robot navigation in a dry sewer test and results is shown in section 4.4. The experimental results showed high self localization computing performance, 100%, and I conclude the single camera as a vision sensor is suitable for our system. But, I also used stereo camera to observe its performance for navigating, which is described in chapter 5.

In chapter 5, I proposed two stereo matching algorithms and I fused some

parts of first algorithms with laser scanner data to propose a method for navigation of an autonomous sewer inspection robot. In section 5.3, I proposed a new cooperative algorithm using a new matching measure of linear computation for a feature group and the conventional Sum of Squared Differences (SSD) with constraints for a non-feature group. In this algorithm, the reference image is divided into the feature pixel group and the non-feature pixel group. The LC measure, which has similarity with the gradient but requires less computational cost, is used in the feature group, and the conventional SSD with neighboring similarity and other constraints is applied to the non-feature group. The computational time by this algorithm is about 1/5 compared with that by other algorithms such as the conventional SSD (section 5.3.2). In section 5.4, I proposed a fast algorithm using cubic interpolation and providing superior performance for autonomous inspection robots. The proposed algorithm is regarded as a combination of a revised Mayer's algorithm and interpolation. At the outset, an image is divided into many blocks. Then, a combined measure of the Sum of Squared Differences (SSD) and cross-correlation is calculated at only the four corner points of the blocks. A downsampled sewer disparity image is composed of only the corner points. Finally, we extend the downsampled sewer disparity image into a regular-sized disparity image by the cubic interpolation, taking advantage of continuous change of disparities in the sewer environment. The computational time by our algorithm is only 1/20 of those by the conventional algorithms such as the SSD. Hence it is suitable for our real-time sewer vision system (section 5.4.2).

In section 5.5, I presented a method for navigation of an autonomous inspection robot in a sewer pipe system based on detection of landmarks. In this method, location of an autonomous sewer inspection robot in the sewer pipe system is estimated from stereo camera images. The laser scanner data are also used to ensure accurate localization of the landmarks and reduce the error in distance estimation by image processing. The method is implemented and evaluated in a sewer pipe test field using a prototype robot, demonstrating its effectiveness (section 5.6).

# Bibliography

[1] http://www.ocbeachinfo.com/downloads/sewagespill.htm

[2] http://www.city.osaka.jp/toshikankyo/english/information/0101.html

[3] R. Kirkham, P.D. Kearney and K.J. Rogers, "PIRAT - A system for quantitative sewer assessment," *In Proc. Int. Conf. Field and Service Robotics (FSR '99)*, CMU, Pittsburgh (PA), pp. 7-12, 1999.

[4] http://vision.cmit.csiro.au/project/pirat/

[5] H.B. Kuntze and H. Haffner, "Experiences with the development of a robot for smart multisensoric pipe inspection," *In Proc. 1998 IEEE Int. Conf. on Robotics and Automation (ICRA '98)*, pp. 1773-1778, Leuven, Belgium, May 1998.

[6] H.B. Kuntze, D. Schmidt, H. Haffner, and M. Loh, "KARO - A flexible robot for smart sensor-based sewer inspection," *In Proc. 12th Int. No-Dig Conference*, pp. 367-374, Hamburg, 1995.

[7] F. Kirchner and J. Hertzberg, "A prototype study of an autonomous robot platform for sewerage system maintenance," *Autonomous Robots*, 4(4):319-331, 1997.

[8] J. Hertzberg and F. Kirchner, "Landmark-based autonomous navigation in sewerage pipes," *In Proc. First Euromicro Workshop on Advanced Mobile Robots (EUROBOT '96)*, pp. 68-73. Kaiserslautern, Germany, Oct. 1996.

[9] F. Schonherr, J. Hertzberg, and W. Burgard, "Probabilistic mapping of unexpected objects by a mobile robot," *In Proc. of the 1999 IEEE/RSJ Int. Conf. on Intelligent Robots and Systems (IROS '99)*, vol.1, pp. 474-481, 1999.

[10] E. Rome, J. Hertzberg, F. Kirchner, U. Licht, H. Streich and Th. Christaller, "Towards autonomous sewer robots: The MAKRO project," *J. Urban Water*, 1:57-70, 1999.

[11] V. Kepplin, K.U. Scholl, and K. Berns, "A mechatronic concept for a sewer inspection robot," *In Proc. IEEE/ASME Int. Conf. on Advanced Intelligent Mechatronics (AIM '99)*, pp. 724-729, Piscataway, NJ, 1999.

[12] K.U. Scholl, V. Kepplin, K. Berns, and R. Dillmann, "Controlling a multijoint robot for autonomous sewer inspection," *In Proc. 2000 IEEE/RAS Int. Conf. on Robotics and Automation (ICRA 2000). IEEE/RAS*, Piscataway (NJ), San Francisco, April 2000.

[13] W. Kampfer, R. Bartzke and W. Ziehl, "Flexible mobile robot system for smart optical pipe inspection," *Proc. SPIE Conf. Nondestructive Evaluation for Aging Infrastructure and Manufacturing (NDE98)*, San Antonio, Texas, March 1998.

[14] A. Thomas and G. Laszczynski, "New technology for enhanced pipeline evaluation," *Proc. of the 1997 ASCE Conf. on Trenchless Pipeline Projects*, pp. 291-297, Boston, MA, USA, June 1997.

[15] J. Biery, A. Ratliff and S. Hall, "Evaluation of 70-year-old non-reinforced concrete sewers," *Proc. of the 1998 Pipeline Division Conference*, pp. 318-327, San Diego, CA, USA, 1998.

[16] J. M. Makar, "Diagnostic techniques for sewer systems," *Journal of Infrastructure Systems*, Nr.2, pp. 69-78, June 1999.

[17] N. K. Opara, R.D. Wooda and N. Shayea, "Nondestructive testing of concrete structures using the rayleigh wave dispersion method," *Anerican Concrete Institute Materials Journal 93*, Nr.1, pp. 75-86, 1996.

[18] T. Price, "Inspecting buried plastic pipe using a rotating sonic caliper," *Proc. of the Second Int. Conf. on Advances in Underground Pipeline Engineering*, Bellevue, Washington, June 1995.

[19] D. Daniels and D. Schidt, "The use of ground probing radar technologies for non-destructive testing of tubes," *Int. Symposium of Nondestructive Testing in Civil Engineering*, pp. 429-436, Berlin, Germany, 1995.

[20] L. Peters, J. Daniels and J. Young, "Ground penetrating radar as a subsurface environmental sensing tool," *Proc. of the IEEE Int. Converence on Robotics and Automation*, pp. 1802-1822, 1994.

77

[21] A. Benson, "Applications of ground penetrating radar in assessing some geological hazards," *Journal of Applied Geophysics 33*, Nr.1-3, 1995.

[22] Material provided by Sewer System Administration Dept., City of Kitakyushu, Japan.

[23] W. Durbeck, "Stand der eigenkontrollverordnung in den landern der bundesrepublik deutschland aus der sicht der industrie," *Dokumentation 4. Int. Kongress Leitungsbau*, Hamburg, Germany, pp. 153-166, Oct. 1994.

[24] M. Keding,S. Riesen and van Esch , "Der zustand der offentlichen Kanalisation in der bundesrepublik deutschland," *Ergebnisse der ATVUmfrage 1990*, Korrespondenz Abwasser, Nr. 10, pp. 1148-1153, 1990.

[25] U. Rudolph and J. Wellnitz, "Zustand und sanierungsbedarf der abwasserkanale in den neuen bundeslandern," *Korrespondenz Abwasser*, Nr. 12, pp. 1625-1630, 1991.

[26] M. Browne, M. Dorn, R. Ouellette, T. Christaller and S. Shiry, "Wavelet entropy-based feature extraction for crack detection in sewer pipes," *Proc. of the 6th Int. Conf. on Mechatronics Technology*, Kitakyushu, Japan, pp. 202-206, 2002.

[27] Nicholas J.Carino, "Concrete technology - past, present and future," ACI SP 144-30, American Concrete Institute, Detroit, MI, pp. 623-678, 1994.

[28] G.E. Stavroulakis and H. Antes, "Nondestructive elostatic identification of unilateral cracks through BEM and neural networks," *Computational Mechanics 20*, Springer Verlag, pp. 439-451, 1997.

[29] A. Bernatzki, W. Eppler and H. Gemmeke, "Interpretation of neural networks for classifi- cation Tasks," *Proc. of EUFIT*, Aachen, Germany, 1996.

[30] S. Yoshimura, G. Yagawa, A. Oishi and K. Yamada, "Neural network based inverse analysis for defect identification with laser ultrasonics," *Key Engeneering Materials*, vols. 145-149, Trans Tech Publications, Switzerland, pp. 443-452, 1998.

[31] A. Mojsilovic, M. Popovic, A. Neskovic and A. Popovic, "Wavelet image extension for analysis and classification of infarcted myocardial tissue," *IEEE Trans. Biomedical Engineering*, vol. 44, no. 9, Sept. 1997.

[32] P. Gunatilake, M. W. Siegel, A. G. Jordan and G. W. Podnar, "Image understanding algorithms for remote visual inspection of aircraft surfaces," *Proc. of the SPIE Conf. on Machine Vision Applications in Industrial Inspection V*, San Jose, SPIE v. 3029, pp. 2-13, Feb. 1997.

[33] Japan sewage works association, "A sewer maintenance indication-first part," pp. 124-125, Aug. 2003.

[34] J. Hertzberg and F. Kirchner, "Landmark-based autonomous navigation in sewerage pipes," *the First EuromicroWorkshop on Advanced Mobile Robots (EUROBOT '96)*, IEEE Press, Los Alamitos, CA, Kaiserslautern, Germany, Oct. 1996.

[35] F. Schonherr, J. Hertzberg and W. Burgard, "Probabilistic mapping of unexpected objects by a mobile robot," *the 1999 IEEE/RSJ Int. Conf. on Intelligent Robots and Systems (IROS '99)*, Vol. 1, IEEE Press, Piscataway, NJ, Kyongju, Korea, Oct. 1999.

[36] L. Paletta, E. Rome and A. Pinz, "Visual object detection for autonomous sewer robots," *the 1999 IEEE/RSJ Int. Conf. on Intelligent Robots and Systems (IROS '99)*, Vol. 2, IEEE Press, Piscataway, NJ, Kyongju, Korea, Oct. 1999.

[37] G. Campbell, K. Rogers and J. Gilbert, "PIRAT - A system for quantitative sewer assessment," *the 12th Int. No-Dig Conference*, Messe und Congress GmbH, Hamburg, Germany, Sept. 1995.

[38] T. Clarke, "The development of an optical triangulation pipe profiling instrument," *Optical 3-D Measurement Techniques III - Applications in inspection, quality control and robotics*, Wichmann, Karlsruhe, Vienna, Oct. 1995.

[39] D. Scharstein and R. Szeliski, "A taxonomy and evaluation of dense two-frame stereo correspondence algorithms," *Int. Journal of Computer Vision*, vol.47, pp. 7-42, 2002.

[40] D. Comaniciu and P. Meer, "Mean shift: A robust approach toward feature space analysis," *IEEE Trans. Pattern Analysis and Machine Intelligence*, vol. 24, no. 5, May 2002.

[41] D. Scharstein, "Matching images by comparing their gradient fields," *Proc. Int. Conf. Pattern Recognition*, vol. 1, pp. 572-575, 1994.

[42] D. Scharstein, "View synthesis using stereo vision," *Springer Press*, pp. 114-120, 1999.

[43] D. Marr and T. Poggio, "Cooperative computation of stereo disparity," *Science*, vol. 194, pp. 209-236, 1976.

[44] D. Marr and T. Poggio, "A computational theory of human stereo vision," *Proc. Royal Soc. London B*, vol. 204, pp. 301-328, 1979.

[45] http://bj.middlebury.edu/ schar/stereo/web/results.php.

[46] L. Hong and G. Chen, "Segment-based stereo matching using graph cuts," *CVPR*, vol.1, pp. 74-81, 2004.

[47] M. Bleyer and M. Gelautz, "Graph-based surface reconstruction from stereo pairs using image segmentation," *Proc. SPIE*, vol. 5665, 2005.

[48] M. Bleyer and M. Gelautz, "A layered stereo algorithm using image segmentation and global visibility constraints," *Proc. IEEE Int. Conf. on Image Processing*, pp. 2997-3000, 2004.

[49] M. Gong and Y.H. Yang, "Near real-time reliable stereo matching using programmable graphics hardware," *IEEE Proc. CVPR*, pp. 924-931, 2005.

[50] V. Kolmogorov and R. Zabih, "Computing visual correspondence with occlusions using graph cuts," *IEEE Int. Conf. on Computer Vision*, 2001.

[51] J. Sun, H. Y. Shum, and N. N. Zheng, "Stereo matching using belief propagation," *IEEE Trans. Pattern Analysis and Machine Intelligence*, vol. 25, no. 7, 2003.

[52] Y. Wei and L. Quan, "Region-based progressive stereo matching," *Proc. Conf. on Computer Vision and Pattern Recognition*, vol.1, pp. 106-113, 2004.

[53] L. Zitnick and T. Kanade, "A cooperative algorithm for stereo matching and occlusion detection," *IEEE Trans. Pattern Analysis and Machine Intelligence*, vol. 22, no. 7, 2000.

[54] S. Forstmann, J. Ohya, Y. Kanou, A. Schmitt, and S. Thuering, "Real-time stereo by using dynamic programming," *Proc. of CVPR Workshop on Real-time 3D Sensors and Their Use*, 2004.

[55] H. Hirschmuller, "Improvements in real-time correlation-based stereo vision," *Proc. of IEEE Workshop on Stereo and Multi-Baseline Vision*, pp. 141-148, 2001.

[56] R. Brockers, M. Hund, and B. Mertsching, "A fast cost relaxation stereo algorithm with occlusion detection for mobile robot applications," *VMV*, 2004.

[57] S. Milan, H. Vaclav and B. Roger, "Image processing, analysis, and machine vision," *Thomson Press*, pp. 448-502, 2002.

[58] H. Mayer, "Analysis of means to improve cooperative disparity estimation," *In Proc. of the ISPRS PIA*, Munich, Germany, 2003.

[59] E. Meijering and M. Unser, "A note on cubic convolution interpolation," *IEEE Trans. on Image Processing*, Vol 12(4), pp. 477-479, 2003.

[60] M. Gong and Y.-H. Yang, "Near real-time reliable stereo matching using programmable graphics hardware," *In Proc. of CVPR*, 2005.

[61] H. Mayer, "Analysis of means to improve cooperative disparity estimation," *ISPRS Conf. on Photogrammetric Image Analysis*, Technical university of Munich, Germany, Sept. 2003.

[62] R. G. Keys, "Cubic convolution interpolation for digital image processing," *IEEE Trans. on Acoust., Speech, Signal Processing*, Vol ASSP-29(6), pp. 1153-1161, 1981.

[63] J. Canny, "A computational approach to edge detection," *IEEE Transactions on Pattern Analysis and Machine Intelligence*, Vol 8, No. 6, Nov. 1986.

[64] "A device and method for fault detection in sewer pipe system," Inventor: A. Ahrary, Japan patent No. 2005-209677, July 2005.

[65] A. Ahrary, L. Tian, S. Kamata and M. Ishikawa, "Navigation of an autonomous sewer inspection robots based on stereo camera images and laser scanner data," *Int. Journal on Artificial Intelligence*, 2007.

[66] A. Ahrary, A. A.F Nassiraei and M. Ishikawa, "A study of an autonomous mobile robot for a sewer inspection system," *Journal of Artificial Life and Robotics*, Vol 11, No. 1, pp. 23-27, Jan. 2007.

[67] A. Ahrary and M. Ishikawa, "A fast stereo matching algorithm using interpolation for sewer inspection robots," *Proc. of the 32nd Annual Conf. of the IEEE Industrial Electronics Society (IECON'06)*, pp. 4060-4065, Nov. 2006.

[68] A. A.F Nassiraei, Y. Kawamura, A. Ahrary, Y. Mikuriya and K. Ishii, "A new approach to the sewer pipe inspection: fully autonomous mobile robot "KANTARO"," *Proc. of the 32nd Annual Conf. of the IEEE Industrial Electronics Society (IECON'06)*, pp. 4088-4093, Nov. 2006.

[69] A. Ahrary and M. Ishikawa, "Sensor fusion for sewer inspection robot navigation," *Proc. of the 37th Int. Symposium on Robotics (ISR'06)*, pp. 1-7, May 2006.

[70] A. Ahrary, Y. Kawamura and M. Ishikawa, "A laser scanner for landmark detection with the sewer inspection robot KANTARO," *Proc. of the IEEE Int. Conf. on System of Systems Engineering (ICSoSE'06)*, pp. 310-315, April 2006.

[71] A. Ahrary and M. Ishikawa, "Self-localization of autonomous sewer robots by using a stereo camera and a laser scanner," *Proc. of the IEEE Int. Conf. on Networking, Sensing and Control (ICNSC'06)*, pp. 1039-1044, April 2006.

[72] A. Ahrary, A. Nassiraei and M. Ishikawa, "A study of an autonomous mobile robot for sewer inspection system," *Proc. of the 11th Int. Symposium on Artificial Life and Robotics (AROB'06)*, pp. 205-208, Jan. 2006.

[73] A. Ahrary, Y. Kawamura and M. Ishikawa, "Fusion of laser scanner data and image data for landmark detection in sewer pipe systems," *Proc. of the 9th Int. Conf. on Mechatronics Technology (ICMT'05)*, pp. 1-5, Dec. 2005.

[74] A. Ahrary and M. Ishikawa, "An automated fault detection system for sewer inspection robots," *Proc. of the 36th Int. Symposium on Robotics (ISR'05)*, WE3C7, pp. 1-5, Dec. 2005.

[75] A. Ahrary, L. Tian, S. Kamata and M. Ishikawa, "An autonomous sewer robots navigation based on stereo camera information," *Proc. of the 17th IEEE Int. Conf. on Tools with Artificial Intelligence (ICTAI'05)*, pp. 628-633, Nov. 2005.

[76] A. Ahrary, L. Tian, S. Kamata and M. Ishikawa, "A cooperative stereo matching algorithm for sewer inspection robots," *Proc. of the IASTED Int. Conf. on Robotics and Applications (RA'05)*, pp. 294-299, Nov. 2005.

[77] A. Ahrary and M. Ishikawa, "Detecting pipe feature points for sewer pipe system based on image information," *Proc. of SPIE Vol.6041, the 10th Int. Conf. on Mechatronics and Information Technology (ICMIT'05)*, pp. 1-5, Sep. 2005.

[78] A. Ahrary and M. Ishikawa, "Visual fault detection for autonomous sewer robots," *Proc. of the 20th Int. Technical Conf. on Circuits/Systems, Computers and Communication (ITC-CSCC'05)*, pp. 201-202, July 2005.